Inorganic Chemistry

Article

pubs.acs.org/IC

Commensurate Superstructure of the {Cu(NO$_3$)(H$_2$O)}(HTae)(Bpy) Coordination Polymer: An Example of 2D Hydrogen-Bonding Networks as Magnetic Exchange Pathway

Roberto Fernández de Luis,*[,†] Edurne S. Larrea,[‡] Joseba Orive,[∥] Luis Lezama,[†,§] and María I. Arriortua*[,†,‡]

[†]Basque Center for Materials, Applications & Nanostructures (BCMaterials), Technological Park of Zamudio, Camino de Ibaizabal, Bndg. 500-first, 48160 Derio, Spain

[‡]Departamento de Mineralogía y Petrología, Facultad de Ciencia y Tecnología and [§]Departamento de Química Inorgánica, Universidad del País Vasco, UPV/EHU, 48940 Leioa, Spain

[∥]Departamento de Ciencia de los Materiales, Facultad de Ciencias Físicas y Matemáticas, Universidad de Chile, Av. Beauchef 851, Santiago 8370448, Chile

Supporting Information

ABSTRACT: The average and commensurate superstructures of the one-dimensional coordination polymer {Cu(NO$_3$)(H$_2$O)}(HTae)(Bpy) (H$_2$Tae = 1,1,2,2-tetraacetylethane, Bpy = 4,4′-bipyridine) were determined by single-crystal X-ray diffraction, and the possible symmetry relations between the space group of the average structure and the superstructure were checked. The crystal structure consists in parallel and oblique {Cu(HTae)(Bpy)} zigzag metal−organic chains stacked along the [100] crystallographic direction. The origin of the fivefold *c* axis in the commensurate superstructure is ascribed to a commensurate modulation of the coordination environment of the copper atoms. The commensurately ordered nitrate groups and coordinated water molecules establish a two-dimensional hydrogen-bonding network. Moreover, the crystal structure shows a commensurate to incommensurate transition at room temperature. The release of the coordination water molecules destabilizes the crystal framework, and the compound shows an irreversible structure transformation above 100 °C. Despite the loss of crystallinity, the spectroscopic studies indicate that the main building blocks of the crystal framework are retained after the transformation. The hydrogen-bonding network not only plays a crucial role stabilizing the crystal structure but also is an important pathway for magnetic exchange transmission. In fact, the magnetic susceptibility curves indicate that after the loss of coordinated water molecules, and hence the collapse of the hydrogen-bonding network, the weak anti-ferromagnetic coupling observed in the initial compound is broken. The electron paramagnetic resonance spectra are the consequence of the average signals from Cu(II) with different orientations, indicating that the magnetic coupling is effective between them. In fact, X- and Q-band data are reflecting different situations; the X-band spectra show the characteristics of an exchange *g*-tensor, while the Q-band signals are coming from both the exchange and the molecular *g*-tensors.

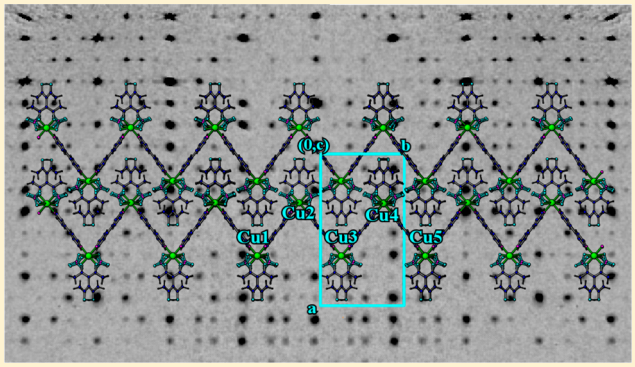

INTRODUCTION

There has been extensive interest in the synthesis and design of new coordination polymers[1] because of their potential applicability in different areas, such as molecular magnetism,[2] molecular recognition and sensing,[3] thermal properties, and[4] protonic conductivity,[5] among others.[6] During the last 20 years, a vast number of structural architectures and fascinating properties has been described in this research field.[7] One interesting crystal engineering approach to construct new coordination polymers is the selection of metal chelating groups different from the commonly used carboxylate-, imidazole-, and/or pyridine-based ligands.[8] In this regard, the *β*-diketonates, and concretely the metal *β*-diketonates, have been under investigation for a long time, and have been recently started to be used as structural building blocks in coordination polymers.[9] Inspired by this strategy, several dimeric, triangular, and rectangular molecular cages and boxes have been obtained based on diketonate-functionalized benzene and naphthalene ligands.[10] These discrete porous cages are endowed with an interesting H$_2$ adsorption capacity, as well as with the ability to host amines, pyridine, and even fullerene molecules.[11] Moreover, for Cu$_2$(o-pba)$_2$ dimeric rings reported by Pariya et al.[12] a color response to the incorporation of

Received: May 16, 2016
Published: November 2, 2016

DOI: 10.1021/acs.inorgchem.6b01199
Inorg. Chem. 2016, 55, 11662−11675

different solvents within the crystal structure has been observed. Another interesting strategy is the incorporation of β-diketonate and cyano groups in the same organic connector, for instance, 3-cyanoacetylacetonate and 3-(3-cyanophenyl)-acetylacetonate molecules.[13] The combination of M(II)-acetylacetonate and M(III)-acetylacetonate building blocks linked through the cyano groups across a second metal center is a very intelligent approach for the design of coordination polymers based on two- and three-connected units.[14]

Among the β-diketonate based connectors, there are few examples of coordination polymers constructed solely from 1,1,2,2-tetraacetylethane (hereafter (H_2Tae)) ligand.[15] Despite the fact that the combination of metal−Tae building blocks and pyridine-based bridging ligands seems to be a good strategy to obtain high-dimensional coordination polymers, the main studies have been focused on the use of chelating ligands, such as 2,2′-bipyridine, 1,10-phenanthroline, or di-2-pyridylamine.[16] Indeed, as far as we know, only one three-dimensional (3D) architecture based on M-Tae-pyridinic ligands has been reported, namely, the three concomitant supramolecular isomers $[Cu_2(Tae)(4,4'\text{-Bpy})_2]^{2+}$ $[(NO_3)_2]^{2-}$ studied by Luisi et al.[17] Delving into the Cu-Tae-4,4′-Bpy system, we obtained the one-dimensional (1D) $\{Cu(NO_3)(H_2O)\}(HTae)(Bpy)$ coordination polymer. Herein, we describe the average orthorhombic crystal structure and the monoclinic commensurate superstructure, along with the impact of the commensurability in the magnetic properties.

Several examples of commensurate[18] and incommensurate[19] superstructures in coordination polymers have been previously reported. The origin for the commensurate and incommensurate order must be considered in each concrete structure, but three main reasons can be quoted: (i) order−disorder transitions, (ii) modulation due to different arrangements and/or orientations of the building blocks, and (iii) occupational modulation. Examples of order−disorder modulation range from dynamical disorder of organic molecules frozen at low measurement temperatures[19] to order−disorder of high spin−low spin Fe(II) in coordination compounds.[20] The $[Ni(MeCN)(H_2O)_2(NO_3)_2]\cdot$(15-crown-5)·MeCN compound reported by Siegler et al. is an example of temperature four phase sequence structural transition due to the reorientation of their building units.[21] Modulation of the occupancy factor for the water molecules located within the pores of lanthanide coordination polymers have been previously reported by Cepeda et al.,[18] but, in this case, the modulation does not affect the coordination environment of the metal centers. The studies performed in commensurable/incommensurable adsorption of different gases in zeolites and MOFs usually involve occupational and positional modulation of the gas molecules located with the pores of the crystal structures.[22] But, in the specific case of the studied coordination polymer, the superstructure is based on the modulation of the coordination environment of Cu(II) metal centers, and concretely, due to the coupled commensurate modulated occupancy of coordinated water molecules and nitrate groups.

As several materials reported before, the studied compound suffers an irreversible structural transformation due to the loss of coordinated water molecules. The spectroscopic and magnetic properties of the initial hydrated phase $\{Cu(NO_3)(H_2O)\}(HTae)(Bpy)$ (hereafter CuHTaeBpy_RT) and the anhydrous compound $\{Cu(NO_3)\}(HTae)(Bpy)$ (hereafter CuHTaeBpy_HT) have been studied. In addition to the crystallographic study, the thermal, spectroscopic, and magnetic properties of the hydrated (CuHTaeBpy_RT) and anhydrous (CuHTaeBpy_HT) compounds reveal the importance of the hydrogen-bonding network within the crystal structure, both in the thermal response of the crystal framework[23,24] and in the establishment of magnetic exchange pathways. It is well-known that the magnetic interaction between metal centers in coordination polymers depends strongly on the number of uncoupled electrons of the metal centers, the bond distances and angles between them, and the magnetic pathway through bridge atoms, anions, or molecules. Despite the weak nature of the hydrogen bonds, and the long distances of metal centers linked through hydrogen-bonding pathways in comparison with M−O−M bridges, it is well-established that they are an effective magnetic exchange pathway, even in coordination polymers with weak magnetic cations, such as Cu(II) (S = 1/2).[25]

EXPERIMENTAL SECTION

Materials and Methods. Commercially available reagent-grade chemicals were purchased from Sigma-Aldrich and used without further purification: 4,4′-bipyridine (Bpy), 1,1,2,2-tetraacetylethane (H_2Tae), $Cu(NO_3)_2\cdot H_2O$, and ethanol (99%). The single crystals of the studied compound were crystallized from saturated ethanolic solutions.

Synthesis. 0.05 mmol (0.0102 gr) of $Cu(NO_3)_2\cdot H_2O$ and 0.05 mmol (0.0099 gr) of H_2Tae were dissolved in 12 mL of ethanol at 80 °C. After dissolving the H_2Tae ligand, the solution was slowly tempered at room temperature. Finally, 0.1 mmol (0.0158 gr) of Bpy organic ligand was added carefully under stirring. After the addition of the pyridinic ligand, the color of the solution changes from pale lemon-green to dark green, associated with the reorganization of the coordination environment of the copper cations. After 1 d, the single crystals began to crystallize. The single crystals were recovered after one week, once the crystallization process had finished, and they were washed with ethanol and dried at room temperature.

Many crystallization experiments at different conditions (temperature, stoichiometry, solvent, etc), were performed. However, departures from the described conditions give rise to the precipitation of a pale green-yellowish powder (CuTae) together with the studied compound. The fast precipitation of CuTae is also promoted by the increase of the pH of the reaction media by the addition of sodium hydroxide or 1,4-diazabicyclo[2.2.2]octane (dbco). Slight increase of the pH of the media led to the deprotonation of the H_2Tae molecules and the consequent precipitation of CuTae compound, competing with the crystallization of CuHTaeBpy_RT. Therefore, the crystallization of CuHTaeBpy_RT needs slow deprotonation of the H_2Tae ligand. The use of other solvents, such as dimethylformamide, acetone, chloroform, chlorobenzene, or tetrahydrofuran, gives rise to the instant precipitation of different poorly crystalline copper-Bpy coordination compounds. So, the formation of CuHTaeBpy_RT is also solvent-dependent. The fast precipitation of both Cu(Tae) and copper-Bpy coordination compounds involves very small single crystals and broad diffraction maxima. Jointly, these two characteristics hinder the solution of their crystal structures by means of single-crystal or powder X-ray diffraction.

Single-Crystal X-ray Diffraction. First, a standard short program was used to obtain the crystal lattice and to confirm the quality of the crystal from a few diffraction images. Once the unit cell and the quality of the single crystal were determined, the data collection of the complete Ewald sphere was performed. Diffraction data were collected on an Agilent Supernova single source diffractometer with Mo Kα radiation at 100 K. Data reduction was done with CrysAlis RED program.[26] The diffraction data were corrected for Lorentz and polarization effects,[27] as well as for the absorption, taking into account the crystal shape and size. The structure was solved by direct methods (SIR-2011[28]) and refined by the full-matrix least-squares procedure based on F^2, using SHELXL 97[29] computer program belonging to WINGX software package.[30] The scattering factors were taken from

DOI: 10.1021/acs.inorgchem.6b01199
Inorg. Chem. 2016, 55, 11662−11675

the International Tables for Crystallography.[31] Details of crystal data, intensity collection, and some features of the structural refinement of both the average and superstructure are reported in Table 1. A complete description of the crystal structure refinements and the average and the superstructure crystallographic relationship can be found in the Supporting Information.

Table 1. Crystal Data and Structure Refinement of the Orthorhombic Average and Monoclinic Superstructures

compound	CuHTaeBpy average structure	CuHTaeBpy superstructure
formula	$C_{20}H_{21}CuN_3O_8$	$C_{100}H_{105}Cu_5N_{15}O_{40}$
Fw (g/mol)	494.95	2474.68
crystal system	orthorhombic	monoclinic
color	green	green
space group, No.	*Pnna*, 52	$P2_1/n$, 14
a (Å)	23.2967(6)	23.282(1)
b (Å)	13.0779(3)	13.0700(7)
c (Å)	6.9267(1)	34.631(2)
β (deg)		90.084(4)
Z, $F(000)$, T (K)	4, 1020, 100	4, 5100, 100
μ (mm^{-1})	1.08	1.09
crystal size (mm)	0.16 × 0.13 × 0.08	0.16 × 0.13 × 0.08
radiation (λ(Å))	0.710 73	0.710 73
No. reflns	2449	24 012
reflns. ($I > 2\sigma(I)$)	1724	9495
h, k, l intervals	$-25 \geq h \geq 31$	$-26 \geq h \geq 31$
	$-17 \geq k \geq 16$	$-16 \geq k \geq 17$
	$-9 \geq l \geq 9$	$-46 \geq l \geq 45$
R(int), $R(\sigma)$	0.061, 0.1796	0.127, 0.5055
$R1$, $wR2$(obs) ($I > 2\sigma(I)$)	0.0653, 0.1550	0.1084, 0.2495
$R1$, $wR2$(all)	0.0946, 0.1758	0.2329, 0.3276
GOF	1.05	1.034
No. parameters/ restraints	153, 12	676, 4
l. diff. peak ($e \cdot Å^{-3}$)	1.05	1.659
l. diff. hole ($e \cdot Å^{-3}$)	−1.52	−0.954

Characterization. The synthesized samples were characterized by powder X-ray diffraction. The data were recorded in a Bruker D8 Advance Vário diffractometer (Cu Kα_1 radiation), 2θ range = 5−70°, step size = 0.015°, exposure time = 10 s per step at room temperature. The Rietveld refinements were performed with the both average and superstructure models. All the refinements were performed with Fullprof Suite software package.[32] Despite the fact that the crystal structures were too complex to perform a refinement of any structural parameter, the use of atomic coordinates allowed the introduction of real intensities into the refinement (Figure S1). This point made more reliable the obtained cell and profile parameters than those obtained from a pattern matching analysis, especially for the large crystallographic cell of the modulated structure.

The percentages of the elements were calculated from C, N, H elemental analysis. Exp: H 4.66(7) %, C 48.6(6) %, and N 8.61(5) %; Theor: H 5.05%, C 48.14%, and N 8.42%. The density could not be determined, because the single crystals are dissolved by the organic solvents usually employed to determine this physical property. The infrared spectra were recorded on a Jasco FT/IR-6100 spectrometer with pressed KBr pellets (400−4000 cm^{-1}). Diffuse reflectance UV−vis spectra of solid samples were registered at room temperature on a Varian Cary 50000 spectro-photometer in the 50 000−4000 cm^{-1} range.

Physical Measurements. The temperature-dependent powder X-ray diffraction in air atmosphere were performed on a Bruker D8 Advance Vantec diffractometer (Cu Kα radiation) equipped with a variable-temperature stage HTK2000 for the measurements performed in the 30 to 400 °C temperature range (2θ range = 9−30°, step size = 0.01°, exposure time = 0.5 s per step). The thermal evolution of the cell parameters for the initial phase was obtained from cyclic Rietveld refinement. The difference between the Rietveld refinement with the average and the commensurate models lies on the fit of several little intense diffraction maxima. In the specific case of the X-ray diffraction patterns of the thermodiffractometry these little intense maxima were not clearly observed, because the technique is focused on the fast acquisition of the data instead of the accuracy. Taking these facts into account the average structural model was chosen to perform the cyclic Rietveld refinement. All the maxima were indexed, in spite of some problems in the fitting of the intensities due to the preferred orientation of the sample.

Thermal analyses were performed in air atmosphere, up to 500 °C, with a heating rate of 5 °C min^{-1} on a Netzsch Sta Simultaneous DSC-TGA. Electron paramagnetic resonance (EPR) powder spectra were recorded on a Bruker ESP300 spectrometer (X- and Q-bands) equipped with Oxford low-temperature devices (magnetic field calibration: NMR probe; determination of the frequency inside the cavity: Hewlett-Packard 5352B microwave frequency counter). The magnetic measurements were performed on a Quantum Design MPMS-7 SQUID magnetometer in the temperature range of 5−300 K. The magnetic field was 0.1 T, a value in the range of linear dependence of magnetization versus magnetic field, even at 5.0 K. The magnetic and spectroscopic measurements were performed both for the as-synthesized sample (CuHTaeBpy_RT) and after dehydrating it at 125 °C during 30 min (CuHTaeBpy_HT).

RESULTS AND DISCUSSION

{Cu(NO$_3$)(H$_2$O)}(HTae)(Bpy) Average and Superstructures. The analysis of the reciprocal space reveals the existence of a fivefold commensurate crystal structure along the "c*" parameter. Figure 1 shows the reciprocal space projection along the b* axis and the hkl layers related with the supercell. The average unit cell can index the main ($hk0$) and ($hk1$) reflections; however, a fivefold c* parameter (q vector = (0, 0, 0.4)) along the [001]* direction is needed to index the less intense satellite reflections.

In addition, the data collection recorded at room temperature reveals that the superstructure becomes incommensurate, with a propagation vector along the c* direction of q = (0, 0, 0.378). Further studies are needed to describe the commensurate and incommensurate crystal structures with four-dimensional superspace groups and to discover the origin of the commensurate to incommensurate structural transition. In this study, the efforts are focused on the description of average and modulated structures, suggesting some possible reasons for the incommensurability of the crystal structure at room temperature. Future studies focused on the structural transition from a commensurate to an incommensurate structure will be reported once the structures are properly described in the fourth dimensional space.[33]

The asymmetric units for the average crystal structure and the superstructure are depicted in Figures 2a,b, respectively. The asymmetric unit of the average crystal structure contains a half of Bpy and HTae molecules, one copper atom lying on a special position, and a half of one nitrate group disordered in two positions. Moreover, a half of coordinated water molecule is disordered and located in the same position that the O1A and O1B atoms belonging to the nitrate anion. The Cu(II) cation is linked to two nitrogen atoms and two oxygen atoms in the equatorial plane, belonging to two Bpy and one HTae ligands, respectively. The disordered nitrate and coordinated water molecules complete the octahedral coordination environment. The symmetry of the *Pnna* space group describes

DOI: 10.1021/acs.inorgchem.6b01199
Inorg. Chem. 2016, 55, 11662−11675

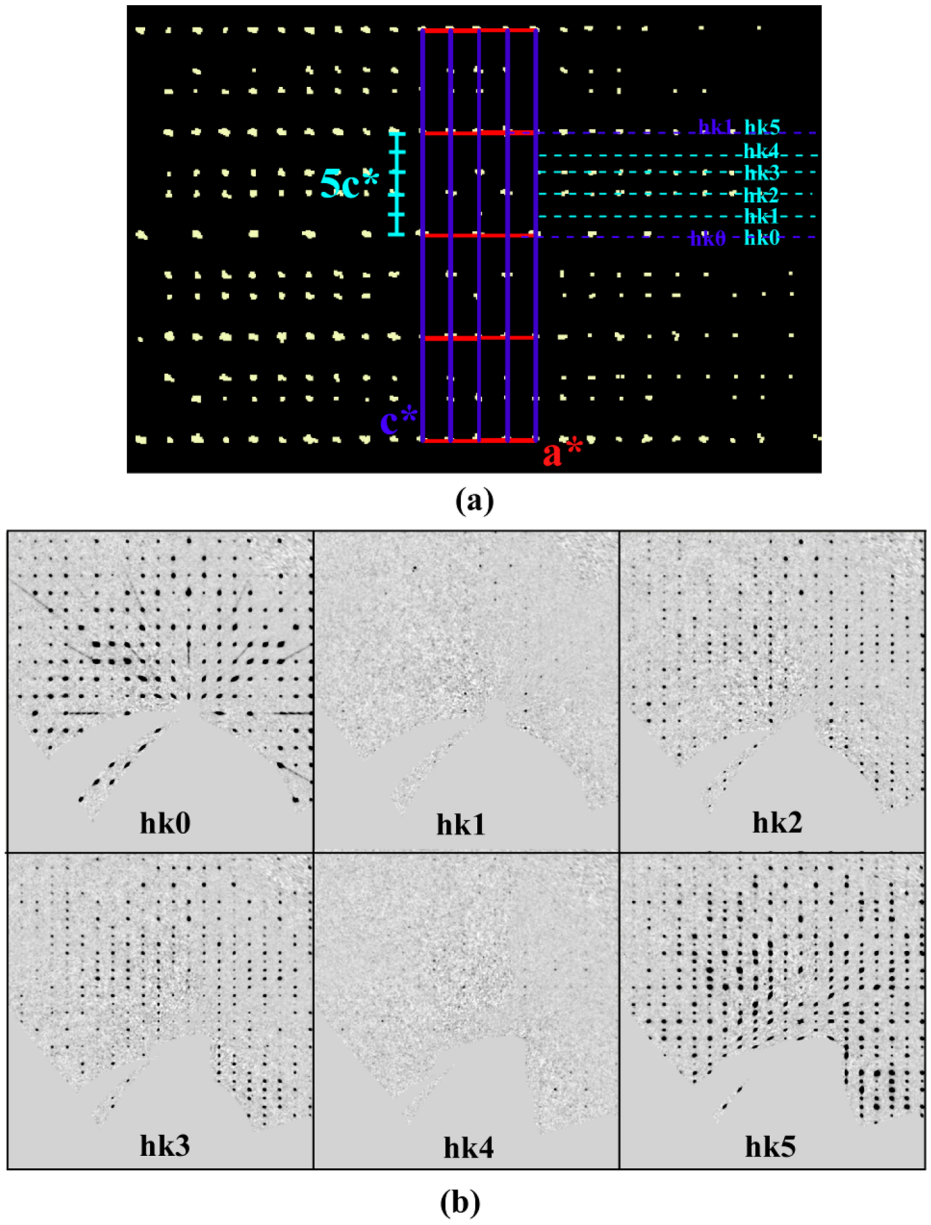

Figure 1. (a) A view of the Ewald sphere along the [010]* crystallographic direction. (b) Reconstruction of the (*hkn*) planes of the reciprocal space. The *hkl* planes were indexed based on the fivefold *c* axis of the supercell.

perfectly the crystal structure of the compound but imposes a random disorder of the nitrate anions and water molecules, instead of the long-range order observed in the superstructure. In this regard, the asymmetric unit of the superstructure contains five crystallographically independent copper atoms, five Bpy, and five HTae molecules (Figure 2b). In this description, the coordination environment of the copper atoms is not equal as in the average structure. Depending on the location of the nitrate groups and the coordinated water molecules in the axial positions of the Cu(II) octahedra, three different coordination environments can be distinguished. The Cu(1) and Cu(4) cations are linked to two coordinated water molecules, the Cu(2) and Cu(5) to two nitrate groups, while the Cu(3) cation is bonded to one nitrate group and one water molecule.

Both the average and the superstructure can be described as a one-dimensional coordination polymer of copper cations linked through Bpy linkers, giving rise to zigzag metal−organic chains. The coordination environment of the copper atoms is completed by one HTae molecule acting as a chelating ligand and the aforementioned nitrate and coordination water molecules.

Tables 2 and 3 summarize the selected bond distances and angles for the average and superstructures. In both structures, the coordination environment of the copper atoms can be described as an axially elongated octahedron. The equatorial plane contains two oxygen and two nitrogen atoms belonging to one HTae and two Bpy organic molecules. The axial positions of the octahedra are occupied by nitrate or coordinated water molecules. The Cu−O_{Tae} bond distances are the shortest ones, with values ranging from 1.882(6) Å, for Cu5−O17, to 1.909(6) Å for Cu1−O2. The Cu−N_{Bpy} bonds are slightly longer with a maximum value of 2.022(6) Å, for Cu2−N3, and a minimum distance of 1.990(7) Å, for Cu3−N5. The axial elongated Cu−O_w and Cu−$O_{Nitrate}$ bonds take values from 2.517(8) Å, for Cu5−O12A, to 2.604(9) Å for Cu3−O9A.

DOI: 10.1021/acs.inorgchem.6b01199
Inorg. Chem. 2016, 55, 11662−11675

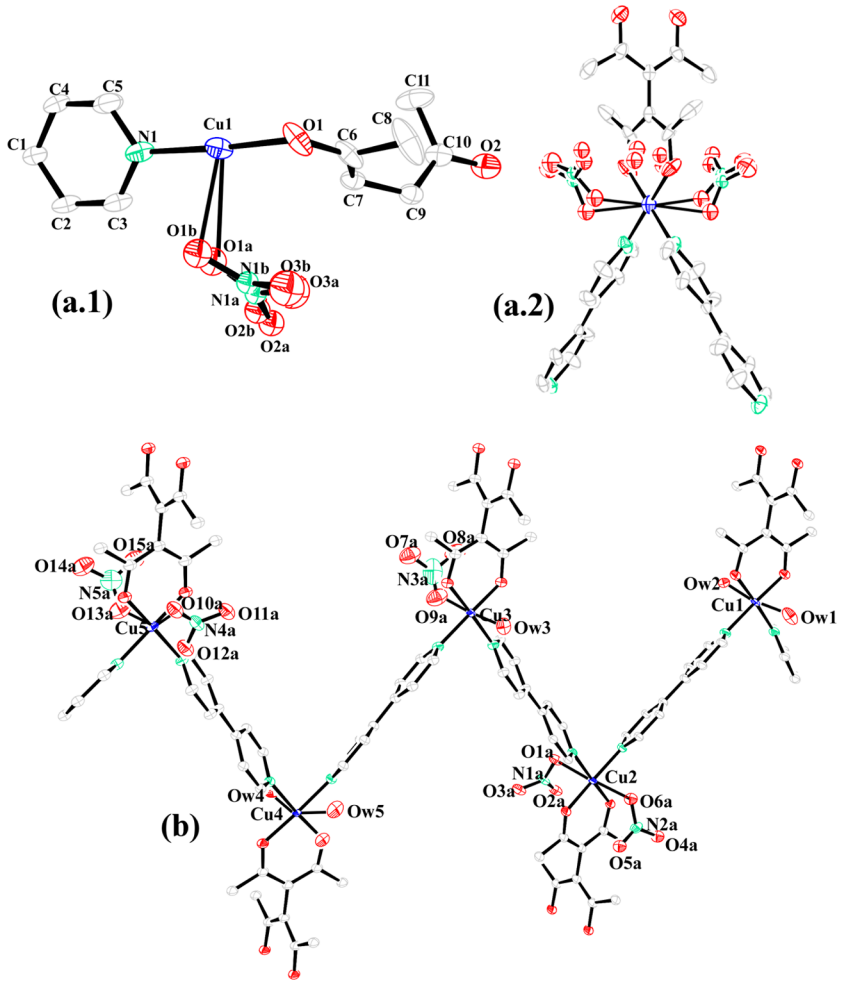

Figure 2. Asymmetric unit (a.1) and fundamental building blocks (a.2.) of the average crystal structure. (b) Superstructure asymmetric units of CuHTaeBpy_RT compound (50% probability thermal ellipsoids). Hydrogen atoms were omitted for clarity.

The Cu−O_w and Cu−$O_{Nitrate}$ interatomic distances are appreciably longer than the bond lengths in the equatorial positions but within the range of weak covalent interactions termed "semi-coordination".[34] The bond valence calculations agree with a 2+ valence for the copper atoms if the contribution of the Cu−O and Cu−O_W bonds are considered into the coordination sphere of the Cu(II) atoms (Table 3).[35] The *trans* and *cis* angles of the copper octahedron are near to the ideal values of 90° and 180° of a regular octahedron. Indeed, continuous shape measures of the metal coordination environments indicate that Cu(II) coordination environments are very near to the ideal octahedron geometry, with values for $S(O_h)$ and $S(D_{3h})$ of 16 and 2, respectively. (Figure S2).[36]

Regarding the C−C and C−O bond distances of the HTae ligand, two types of bond lengths are found. The first one is associated with the C−C single bonds (ca. 1.49 Å) involving the methyl groups, and the second one is related to the resonant C═C (ca. 1.40 Å) and C═O (ca. 1.30 Å) bonds. One proton is located between the two oxygen atoms of the HTae ligand nonbonded to the Cu(II) cations, with O−H bond distance of ca. 1.22 Å.

The packing of the {Cu(HTae)(Bpy)} metal−organic chains in the *ab* plane is shown in Figure 3. The zigzag chains are parallel stacked. The HTae ligands of one chain point toward the copper cations of the adjacent ones. To visualize more easily the crystal packing of the metal−organic chains, the simplification of the crystal structure was performed with TOPOS software, considering the Cu(II) cations and the Bpy organic ligands as the nodes. The Cu and Bpy nodes are alternatively connected giving rise to the zigzag simplified chains observed in the Figure 4a. As the HTae ligand acts as chelating molecule binding only one copper atom, they are omitted in the simplified model. There are two kind of chains depending on their propagation direction, the [011] and [0−11] chains (green and blue codes, respectively, in Figure 4b). Each sort of chain is stacked in an ABABAB-type sequence along the [100] crystallographic direction (Figure 4c).

The main differences between the average and the superstructure are (i) coordination environment of the copper cations and (ii) the hydrogen bonding established between the coordination water molecules and nitrate groups. In fact, randomly disordered nitrate groups and water molecules described in the average crystal structure do not stand the real hydrogen bonding of the network. It is not possible to calculate the interchain hydrogen bonding because of the disorder of the nitrate groups imposed by the symmetry. The hydrogen bonds obtained from the average structure only involve intrachain interactions. However, the superstructure allows describing the real hydrogen-bonding network. In addition to the intrachain hydrogen bonds, the modulated long-range order of the nitrate and coordinated water molecules generates a two-dimensional (2D) hydrogen-

DOI: 10.1021/acs.inorgchem.6b01199
Inorg. Chem. 2016, 55, 11662−11675

Table 2. Selected Bond Distances (Å) and Angles (deg) for the Average Crystal Structure

Bpy[a] (distances)		HTae[a] (distances)	
C1−N1	1.341(5)	C6−O1	1.273(5)
C1−C2	1.377(6)	C6−C7	1.408(5)
C2−C3	1.385(5)	C6−C8	1.488(6)
C3−C4	1.396(6)	C7−C6^{ii}	1.408(5)
C3−C3^{i}	1.487(8)	C7−C9	1.493(8)
C4−C5	1.362(7)	C9−C10	1.402(5)
C5−N1	1.340(5)	C9−C10^{ii}	1.402(5)
Bpy (angles)		C10−O2	1.300(5)
N1−C1−C2	122.5(4)	C10−C11	1.498(6)
C1−C2−C3	120.4(4)	O2−H1A	1.227(5)
C2−C3−C4	116.5(4)	HTae (angles)	
C2−C3−C3^{i}	122.0(4)	O1−C6−C7	124.8(4)
C4−C3−C3^{i}	121.5(4)	O1−C6−C8	113.5(4)
C5−C4−C3	119.9(4)	C7−C6−C8	121.6(4)
N1−C5−C4	123.5(4)	C6−C7−C6^{ii}	122.6(5)
C5−N1−C1	117.2(4)	C6−C7−C9	118.7(3)
Cu(II) (distances)		C6^{ii}−C7−C9	118.7(3)
Cu1−O1	1.896(3)	C10−C9−C10^{ii}	117.5(5)
Cu1−O1^{ii}	1.896(3)	C10−C9−C7	121.2(3)
Cu1−N1^{ii}	2.008(4)	C10^{ii}−C9−C7	121.2(3)
Cu1−N1	2.008(4)	O2−C10−C9	122.4(4)
Cu1−O1A	2.529(6)	O2−C10−C11	115.7(4)
Cu1−O1B	2.585(6)	C9−C10−C11	121.9(4)
Cu(II) (angles)		C10−O2−H1A	92 (3)
O1−Cu1−O1^{ii}	92.66(18)	nitrate (angles)	
O1−Cu1−N1^{ii}	90.09(14)	O1A−N1A−O3A	129.7(10)
O1^{ii}−Cu1−N1^{ii}	176.40(14)	O1A−N1A−O2A	107.8(7)
O1−Cu1−N1	176.40(14)	O3A−N1A−O2A	120.8(9)
O1^{ii}−Cu1−N1	90.09(14)	O3A^{iii}−O3A−N1A	156.9(11)
N1^{ii}−Cu1−N1	87.3(2)	O1B−N1B−O3B	122.4(8)
N1−Cu1−O1A	92.38(17)	O1B−N1B−O2B	116.6(8)
N1−Cu1−O1B	92.06(17)	O3B−N1B−O2B	120.8(9)
O1−Cu1−O1A	90.27(16)	O3B^{iii}−O3B−N1B	146(3)
O1−Cu1−O1B	89.86(16)		
nitrate (distances)			
N1A−O1A	1.174(8)		
N1A−O3A	1.219(8)		
N1A−O2A	1.277(8)		
N1B−O1B	1.197(8)		
N1B−O3B	1.240(8)		
N1B−O2B	1.266(8)		

[a]Symmetry codes: (i) $-x, -y + 1, -z + 2$; (ii) $x, -y + 1/2, -z + 1/2$; (iii) $-x + 1/2, -y, z$.

bonding network shown in Figure 5a. With the aim of visualizing the connection between the metal−organic chains through the hydrogen bonds the simplification of the crystal structure shown in Figure 5b,c were made. The chains are represented as the copper metal centers linked through the Bpy ligand. For each copper metal center, the coordinated water molecules or the nitrate groups were also represented as single nodes. The 2D hydrogen-bonding net consists of the linkage of parallel metal−organic chains represented in Figure 5b and the connection between the crossed adjacent chains shown in Figure 5c.

Figure 5b depicts the simplified parallel chains and their connectivity through the hydrogen bonds along the [001] direction, which plays a crucial role in the commensurability of the superstructure at low temperature. The connection of the metal−organic chains in this direction follows the Cu(1)−O_w−NO_3−Cu(2)−NO_3−O_w−Cu(4)−O_w−NO_3−Cu(5)−NO_3−O_w−Cu(3)−NO_3−O_w−Cu(1) sequence, as shown in Figure 5b. The connectivity between adjacent crossed chains is given by the Cu(1)−Ow−NO_3−Ow−Cu(5), Cu(2)−NO_3−Ow−Cu(4), and Cu(3)−Ow−NO_3−Cu(3) successions along the [100] direction (Figure 5c). Clearly, the coordination environments of the copper atoms are arranged facing nitrate and coordinated water molecules, promoting the formation of the described hydrogen-bonding patterns. Both the different coordination environments of the copper cations and the hydrogen bonding between them justify the fivefold c^* axis in the commensurate structure. Probably, the origin of the incommensurability at room temperature comes from the distortion of the hydrogen-bonding network, but further insights for clarifying these points are needed.

Similar {Cu-Bpy-L} (L = chelating ligand) metal−organic chains are present in other 1D coordination polymers, but with alanine,[37] adipic acid,[38] 2-pyrazinecarboxylic acid,[39] or aminobenzoic acid[40] as chelating ligands. In the specific case of negatively charged chelating molecules, the positive charge of Cu-Bpy cationic chains is completely or partially compensated. In the latter case, the crystal structure incorporates inorganic anions (nitrate and sulfate groups, among others) balancing the charge of the crystal framework.[41] These species could be coordinated in different degrees to the copper cations or simply located within the pores of the crystal structures. As it has been indicated in the introduction, Luisi et. al[18] obtained three different $[Cu_2(Tae)(4,4'\text{-Bpy})_2]^{2+}[(NO_3)_2]^{2-}$ isomers containing Tae^{-2} ligand acting as connector. Curiously, Cu(II)Bpy chains similar to those present in CuHTaeBpy_RT are observed in these crystal structures, but their connectivity through Tae^{-2} generates three different porous 3D architectures.

The synthesis method for the crystallization of CuHTaeBpy_RT and the 3D compounds reported by Luisi et. al is different. While CuHTaeBpy_RT is obtained as the major product of crystallization by evaporation technique from ethanolic solution, the $[Cu_2(Tae)(4,4'\text{-Bpy})_2]^{2+}[(NO_3)_2]^{2-}$ isomers crystallize as few single crystals by slow diffusion of a methanolic solution of Bpy into a methanolic solution of Tae and copper(II) nitrate across an inverted U-tube bridge. Different isomers are collected from distinct regions of the bridge, suggesting that slight variation on synthetic conditions (concentration, stoichiometry of reagents···) could shift the crystallization pathway.

Thermal and Spectroscopic Properties. The thermogravimetric analysis shows four different steps of weight loss (Figure S3), but the last three are strongly overlapped, so the information acquired from the thermodiffractometric analysis is needed to separate the processes. The first weight loss occurs between room temperature and 130 °C due to a continuous loss of the surface moisture of the sample and coordinated water molecules, (Theor 3.6%, Obs 5.4%). The release of coordinated water molecules is slightly endothermic, as observed in the differential scanning calorimetry (DSC) curve peak. A second weight loss is observed between 130 and 160 °C. This second process is immediately followed by the collapse of the crystal framework due to the loss of Bpy and Tae molecules. It is possible to separate both processes because of (i) the exothermic peak observed in the DSC curve centered at 160 °C and (ii) the information given by the thermodiffractometric analysis, in which the collapse of the crystal

DOI: 10.1021/acs.inorgchem.6b01199
Inorg. Chem. 2016, 55, 11662−11675

Table 3. Copper Coordination Environment Bond Distances (Å) and Bond Valence Calculations for the Orthorhombic Average Structure and Monoclinic Superstructure

average[a]		bond valence	superstructure		bond valence
Cu1−O1	1.896(3)	0.556 28	Cu3−O10	1.894(6)	0.559 29
Cu1−O1^{ii}	1.896(3)	0.556 28	Cu3−O9	1.895(6)	0.557 78
Cu1−N1^{ii}	2.008(4)	0.341 07	Cu3−N5	1.990(7)	0.358 07
Cu1−N1	2.008(4)	0.341 07	Cu3−N6	2.013(7)	0.336 49
Cu1−O1A	2.529(6)	0.100 53	Cu3−O9A	2.604(9)	0.082 085
Cu1−O1B	2.585(6)	0.086 410	Cu3−O3W	2.539(6)	0.097 850
		1.9816			1.9916
superstructure			superstructure		
Cu1−O1	1.898(5)	0.553 28	Cu4−O14	1.889(6)	0.566 90
Cu1−O2	1.909(6)	0.537 07	Cu4−O13	1.894(5)	0.559 29
Cu1−N2	2.000(7)	0.348 52	Cu4−N8	2.000(7)	0.348 52
Cu1−N1	2.015(7)	0.334 68	Cu4−N7	2.012(7)	0.337 40
Cu1−O1W	2.602(6)	0.082 530	Cu4−O4W	2.577(6)	0.088 299
Cu1−O2W	2.547(5)	0.095 757	Cu4−O5W	2.595(6)	0.084 106
		1.9518			1.9845
superstructure			superstructure		
Cu2−O6	1.893(5)	0.560 81	Cu5−O17	1.882(6)	0.577 73
Cu2−O5	1.895(5)	0.557 78	Cu5−O18	1.889(6)	0.566 90
Cu2−N4	2.017(7)	0.332 87	Cu5−N10	2.000(7)	0.348 52
Cu2−N3	2.022(6)	0.328 40	Cu5−N9	2.017(7)	0.332 87
Cu2−O1A	2.545(6)	0.096 276	Cu5−O12A	2.517(8)	0.103 84
Cu2−O6A	2.539(6)	0.097 850	Cu5−O13A	2.567(7)	0.090 718
		1.9740			2.0206

[a]Symmetry codes: (ii) $x, -y + 1/2, -z + 1/2$.

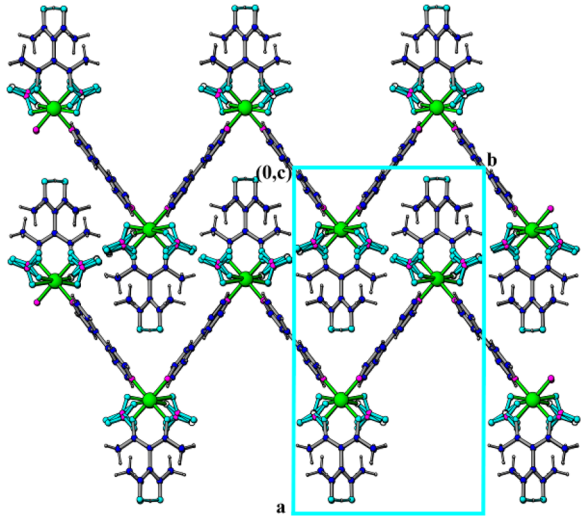

Figure 3. Packing of the {Cu(HTae)(Bpy)} metal−organic chains. View of the CuHTaeBpy_RT average crystal structure in the *ab* plane.

framework starts also at 160 °C. According to the crystal structure and formula unit, upon 130 °C the release of nitrate groups could explain the weight loss observed in this second step (Theor 12.4%, Obs 12.8%). Finally, the loss of the Bpy and Tae organic molecules occurs between 160 and 320 °C. The first stage of the release of the organic molecules is progressive and occurs between 160 and 215 °C. Above this temperature, a sharp and exothermic weight loss is observed up to 245 °C, at which temperature this process is attenuated up to 320 °C. In this last stage (245−320 °C), both the release of Bpy and Tae molecules and the oxidation of Cu atoms occur simultaneously (Theor 67.8% Obs 65.7%).

The temperature-dependent X-ray diffraction experiment indicates that the initial crystal structure is stable up to 100 °C (Figure S4). Above this temperature, the compound is transformed due to the loss of coordinated water molecules. The reduction of the intensity and the increase of the half-width of the diffraction maxima in the dehydrated phase suggest a loss of crystallinity due to the collapse of the 2D hydrogen-bonding network and the reorganization of the crystal structure.[42] The dehydrated phase is stable up to 150 °C. Upon this temperature and until 200 °C, the release of nitrate groups gives rise to a progressive loss of intensity in the X-ray diffraction patterns related to the collapse of the framework.

The thermal evolution of the cell parameters reveals an anisotropic thermal response of the crystal structure (Figure 6). In fact, while "*b*" and "*c*" parameters increase with temperature, "*a*" parameter is reduced. On the basis of previous studies, the thermal behavior of coordination polymers is usually ascribed to the reorientation of rigid blocks.[43] For the studied crystal structure, the thermal expansion can be qualitatively explained taking into account the connection of the copper octahedra through the Bpy organic ligands. A simplified model is shown in Figure S5. It is reasonable to suppose that the distance between the copper atoms linked through the Bpy molecules remains approximately unaltered during the heating process (ca. 11 Å). The elongation of the metal−organic chains could be reached by an increase of Bpy−Cu−Bpy angle (Figure S5). Since the metal−organic chains are oriented in the [011] and [01−1] directions, their elongation generates the expansion of the "*b*" and "*c*" parameters and the reduction of the "*a*" parameter.[44]

It is well worth pointing out the exponential tendency of "*a*" and "*b*" parameters between room temperature and 100 °C. In fact, if the cell parameters obtained at 100 K by single-crystal X-ray diffraction are plotted (see Figure S6), this trend seems to

DOI: 10.1021/acs.inorgchem.6b01199
Inorg. Chem. 2016, 55, 11662−11675

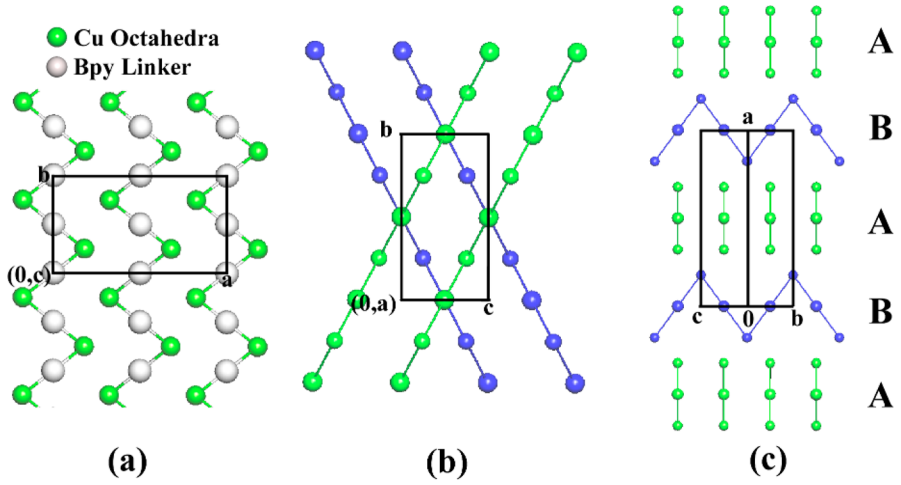

Figure 4. (a) Structure simplification. Green nodes: copper octahedra. Gray nodes: Bpy ligand. (b) Representation of the two types of metal−organic chains (green chains: [011] propagation direction and blue chains: [0−11] propagation direction). (c) ABABA packing of the [011] and [0−11] chains along the [100] crystallographic direction.

be more pronounced above room temperature. This exponential tendency is ascribed to the expansion of hydrogen-bonding network and the closeness to the critical temperature at which the bonded water molecules are released from the crystal framework.

The loss of coordinated water molecules in the structural transformation was also studied by IR and UV−vis spectroscopies. After the structural transformation, the main absorption bands of the IR spectra, except the absorption bands assigned to the vibrational modes of the coordinated water molecules, are retained, so the structural blocks of the crystal structure are maintained after the loss of ccordinated water molecules (Figure S7). Similarly, the UV−vis spectra for CuHTaeBpy_RT and CuHTaeBpy_HT show no appreciable changes in the coordination environment of the Cu(II) cations during the structural transformation (Figure S8).

Electron Paramagnetic Resonance Spectroscopy. X- and Q-band EPR measurements were performed on powdered samples at several temperatures in the range of 5−300 K. The spin Hamiltonian parameters were estimated by comparison of the experimental spectra with those obtained by a computer simulation program working at the second order of the perturbation theory. The parameters were then optimized by the trial-and-error method, and the best-fit results are represented as dashed lines in Figure 7.

The X-band powder EPR spectrum of CuHTaeBpy-RT has the characteristic shape of Cu(II) sites with rhombic symmetry without hyperfine structure (Figure 7a). The main g-values are $g_1 = 2.215$, $g_2 = 2.102$, and $g_3 = 2.056$ ($g_{iso} = 2.127$), remaining practically unchanged from room temperature to 5 K. The calculated exchange tensor parameter G is 2.7,[45] which indicates that the g values obtained from experiment are not equal to the molecular ones and do not reflect the individual geometries of our Cu(II)$N_2O_2H_2O/NO_3$ chromospheres. Two possible explanations are possible for this scenario: (i) a fluxional behavior originated from a dynamic Jahn−Teller effect (elongation-shortening of copper coordination environment along Cu−NO_3 or Cu−O_w bonds within the octahedron)[46] or (ii) the presence of long-range magnetic interactions seem to be the most plausible explanations among all phenomena that could lead to a rhombic signal with collapsed hyperfine structure. The low g_1 value would be in agreement with a 2D fluxional behavior, which should be confirmed by a shift of lowest field signal with decreasing temperature. However, no significant change takes place when down to 5 K; hence, any dynamic Jahn−Teller effect can be dismissed. Therefore, the spectra could be attributed to an exchange g tensor derived from a certain degree of magnetic exchange between magnetically nonequivalent Cu(II) cations along the Cu(Bpy) chain or within the 2D hydrogen-bonding network. It is well-known that rhombic signals are also obtained for magnetically coupled Cu(II) cations with different orientations in the unit cell. In fact, while in the average structure this condition is not fulfilled, for the superstructure the five crystallographically independent Cu(II) cations are not related by inversion centers or translation symmetry, so their magnetic orientations within the unit cell could be also different.[47] Moreover, long-range, weak magnetic interactions between distant Cu(II) atoms have been found to have a clear effect in the EPR spectra. For example, this is the case of [$Cu(py)_2Cl_2$], where Cu(II) atoms are separated by ca. 9 Å and connected by sequences of six consecutive bonds and interactions were found to be coupled on the basis of EPR spectroscopy.[48] For the studied compound, the sharp and intense signal centered at ∼3260 G suggests the existence of a 1D coupled system. The EPR line corresponds to a collective resonance when the exchange interaction (J) between copper ions in different lattice sites is larger than the difference between their Zeeman energies (0.3 cm^{-1} at X-band).

On the Q-band EPR spectrum an additional rhombic signal is observed, with $g'_1 = 2.258$, $g'_2 = 2.069$, and $g'_3 = 2.059$ ($g'_{iso} = 2.129$). Considering that these g-values are molecular ($G = 4.0$), while the average parameter is practically the same in both signals, it can be concluded that the Q-band spectrum shows contributions from both molecular and exchange g tensors. In fact, when the magnetic exchange between the Cu(II) cations is lower than the microwave energy applied in the EPR experiment the magnetic exchange could be overcome, and only the molecular spectra of the Cu(II) cations could be observed. Thus, the observed behavior implies that operating at Q-band the condition $J < |Ng|\mu_B H$ does not hold for any orientation of the magnetic field.

X-band spectrum for the anhydrous phase (CuHTaeBpy_HT) was also recorded (Figure S9). After the dehydration,

DOI: 10.1021/acs.inorgchem.6b01199
Inorg. Chem. 2016, 55, 11662−11675

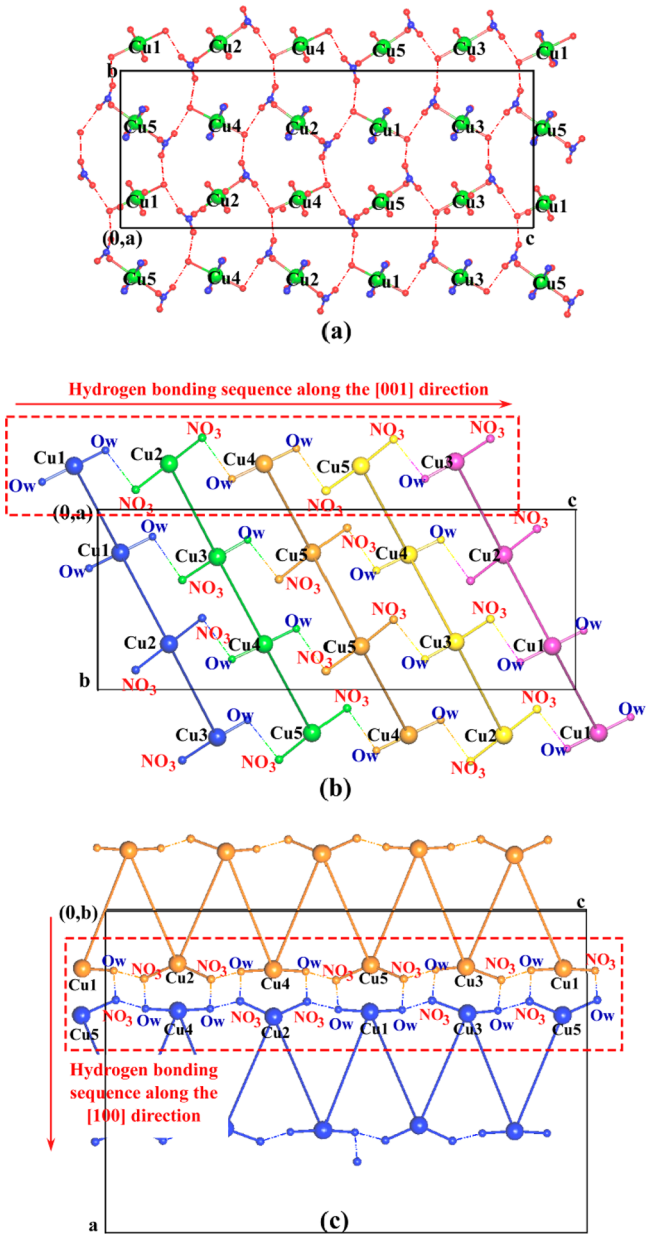

Figure 5. (a) Hydrogen-bonding network in the monoclinic superstructure. (b) Simplification of the metal−organic chains. The crystallographically independent chains were plotted with different colors. The figure highlights the hydrogen-bonding sequence between them along the [001] direction. (c) Hydrogen bonding between two adjacent metal−organic chains along the [100] crystallographic direction.

and the rearrangement of the crystal structure, the three main signals ascribed to the magnetic exchange *g*-tensor are appreciably broadened, in good agreement with the loss of order observed by powder X-ray diffraction. However, the peak related to the g3 exchange tensor retains the sharp and intense absorption signal ascribed to a one-dimensionally coupled copper cation. Despite the loss of order after the dehydration, the Cu-Bpy metal−organic chains are retained after the transformation, being still an effective magnetic exchange pathway.

Magnetic Properties. Magnetic measurements were performed on powdered samples from room temperature to 5 K at a magnetic field of 0.1 T. The thermal evolution of the

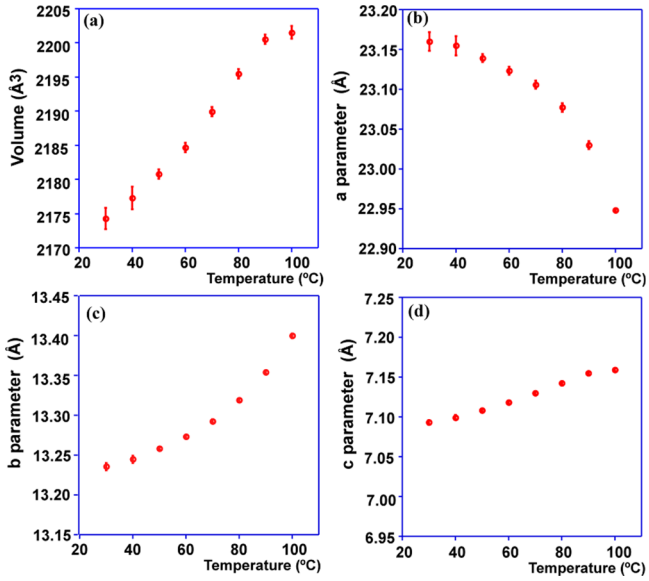

Figure 6. Thermal evolution of the (a) volume (Å^3) and (b) *a* parameter (Å), (c) *b* parameter (Å) and (d) *c* parameter (Å).

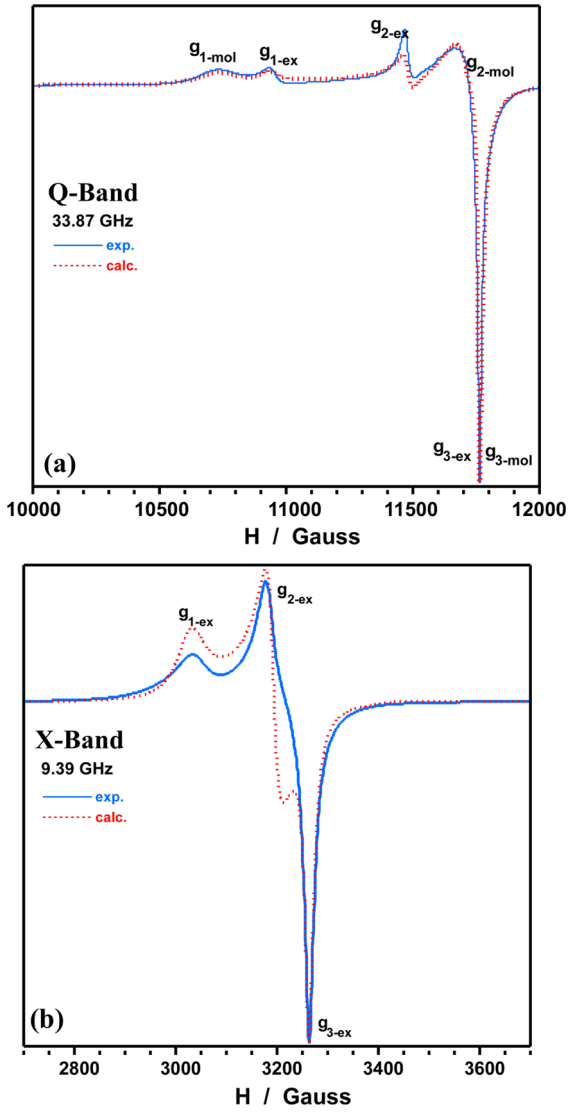

Figure 7. X- and Q-band EPR spectra for CuTaeBpy_RT.

DOI: 10.1021/acs.inorgchem.6b01199
Inorg. Chem. 2016, 55, 11662−11675

χ_m and $\chi_m T$ product for the as-synthesized compound (CuHTaeBpy_RT) and the dehydrated sample (CuHTaeBpy_HT) are shown in Figure 8. While the magnetic

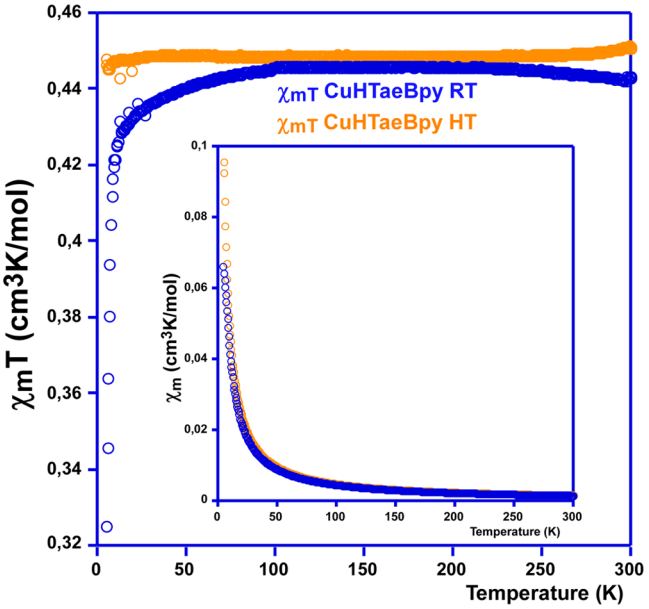

Figure 8. Thermal evolution of χ_m and $\chi_m T$ curves for as-synthesized (CuHTaeBpy_RT) and dehydrated (CuHTaeBpy_HT) compounds.

susceptibility increases from 300 to 5 K for both RT and HT compounds, the $\chi_m T$ product curves show that there is a weak decrease below the Curie temperature, being higher for the RT phase (Figure 8 inset). The decrease on the $\chi_m T$ product for CuHTaeBpy_RT indicates a small anti-ferromagnetic coupling between the copper metal centers below the Weiss temperature. This interpretation was confirmed by the fits of the Curie–Weiss plots, with slightly negative Weiss temperature of $\theta = -0.60$ K for the RT compound and near 0 K ($\theta = 0.02$ K) for the HT one. The obtained Curie constants are very similar for both compounds, 0.447 (RT) and 0.449 (HT) emu K mol^{-1}, and near the expected value for a magnetically isolated Cu^{2+} ($S = 1/2$ with $g > 2$) cation.

If the aforementioned superstructure is taken into account, the shortest distance between copper cations is ca. 11 Å across the Bpy organic ligands, too long to be a magnetically effective exchange pathway. However, the 2D hydrogen bonding between copper atoms through the nitrate groups and coordinated water molecules plays a very important role in the transmission of the magnetic coupling. In this sense, there are two possible magnetic pathways (see Figure 9): *J1* that connects the Cu(II) cations along the [001] direction and *J2* pathway, which involves the metal centers connected along the [010] crystallographic direction. In both of them, copper atoms are hydrogen-bonded through a nitrate group and a coordinated water molecule, Cu–NO_3–H_2O–Cu, with Cu···Cu distances near to 7.00 Å for *J1* and 7.35 Å for *J2*.[49]

All attempts to fit the CuHTeBpy_RT magnetic data to an Ising model for $S = 1/2$ chains (*J1*) with a molecular field term (*J2*) to describe the interchain interactions were unsuccessful. If the molecular term is not taken into account, reasonable g (2.193(1)) and *J1* (−1.73(3) K) values are obtained, but the fit below 100 K deviates appreciably from the experimental data. A 2D Heisenberg model improves the fitting down to 40 K, with similar g 2.1882(7) values and slightly lower *J1* coupling (−0.47(1) K). However, the reduction of the $\chi_m T$ product below 20 K suggests that the anti-ferromagnetic coupling through the hydrogen-bonding network is more complex than the 1D and 2D models used to fit the data (Figure S10). $\chi_m T$ product evolution for CuHTeBpy_HT curves were fitted to the same models used for the room-temperature compound with similar results for both models: $g_{1D} = 2.188(1)$, $g_{2D} = 2.869(7)$,

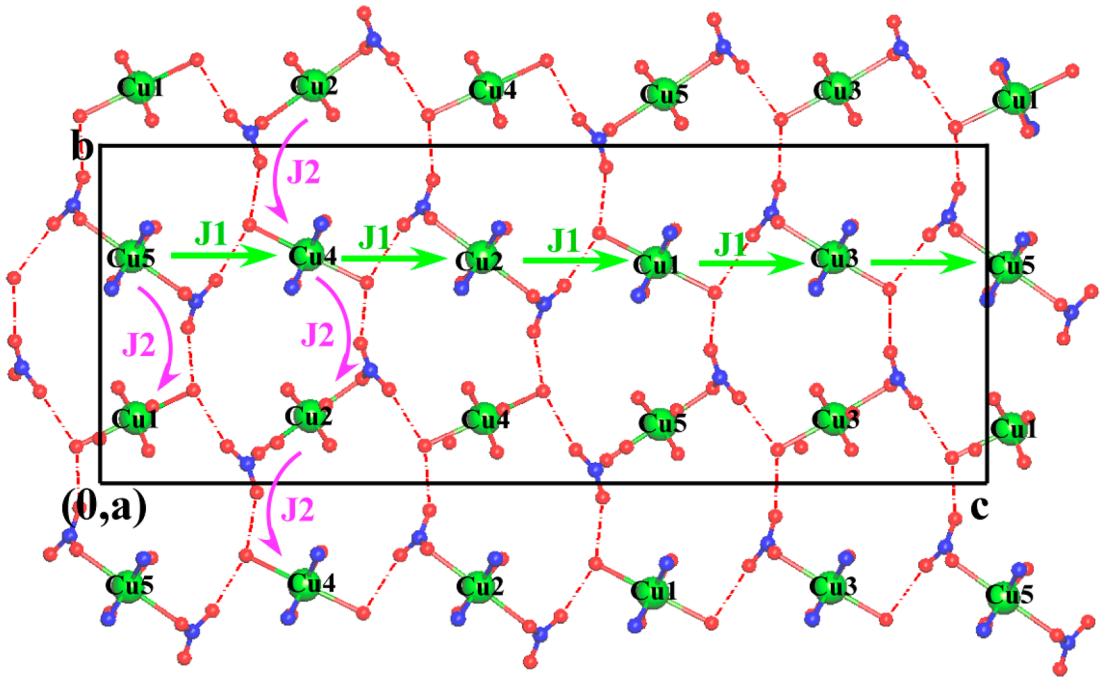

Figure 9. Magnetic exchange pathways between copper cations through the hydrogen-bonding network. *J1* and *J2* with Cu···Cu distances of 7.00 and 7.35 Å involving five connecting atoms Cu–O–N–O–H–O–Cu between copper cations.

DOI: 10.1021/acs.inorgchem.6b01199
Inorg. Chem. 2016, 55, 11662–11675

$J1_{1D}$ = −0.080(4) K, and $J1_{2D}$ = −0.0168(8) K. It is difficult to find out what kind of magnetic exchange pathways are still effective between the copper centers in CuHTeBpy_HT without a structural model, but this little departure from the paramagnetism at low temperatures indicates that the antiferromagnetic coupling is still effective but one order lower than the interactions observed in CuHTeBpy_RT. Therefore, the collapse of the hydrogen-bonding network breaks the antiferromagnetic exchange pathways between the copper atoms.

It is well-known that the hydrogen bonds can be effective magnetic exchange pathways. In fact, several copper compounds exhibiting copper chains connected through hydrogen bonds, and, hence, 1D magnetic coupling, have been reported previously.[50] Even more complex magnetic systems based on magnetic exchange through hydrogen bonds have been also reported, such as 1D intra- and intercoupled chains[51] or dimmers coupled through hydrogen bonds.[52] Nevertheless, in all these cases, there is a clear *J1* exchange pathway with the shortest Cu···Cu distance and a secondary *J2* magnetic exchange pathway, in which the copper atoms are separated by longer distances and more complex magnetic pathways. However, in the specific case of the studied compound the Cu···Cu *J1* and *J2* magnetic superexchange pathways involve the same connectivity and hydrogen-bonding sequence and similar Cu···Cu distances, so one copper atom can interact with four neighbor atoms giving rise to a 2D system. The slight distortion of this 2D net could explain the deviation from the magnetic model at low temperatures.

CONCLUSIONS

The average and commensurate structures are two possible descriptions of the same structural data. The average structure gives us a general picture of the metal−organic chains, their arrangement, and the underlying symmetry of the superstructure, but it does not describe properly the occupational commensurate modulation of the nitrate and water molecules. Indeed, the symmetry of the average structure imposes an unreal disorder in the nitrate groups, not observed in the superstructure. While in other compounds the commensurability or incommensurability come from a distortion of the framework, and the average structure could give an average picture of the modulation, and, in the end, a correct average structural model, in the studied compound the underlying symmetry in the superstructure gives rise to an incorrect disordered average model for the nitrate groups and coordinated water molecules, and hence, to an incorrect hydrogen-bonding scheme. In this case, the structural information extracted from the average model must be interpreted carefully, but it is a very important starting point to solve, refine, and read the real superstructural model.

The fivefold commensurability is the consequence of the commensurate order of the nitrate and coordinated water molecules, which, in turn, is the result of the hydrogen interactions established between them. Of course the Cu−Bpy−Tae organic chains and their arrangement are flexible enough to accommodate the distortion of the net originated by this hydrogen-bonding network.

As in many other supramolecular compounds, the loss of the hydrogen-bonding network gives rise to the collapse of the crystal structure but does not break the fundamental building blocks of the crystal structure, which are still retained in the less crystalline high-temperature phase.

The importance of the hydrogen-bonding network as a magnetic exchange pathway is corroborated by the weak antiferromagnetic coupling of the copper metal centers observed in the magnetic susceptibility of the hydrated compound (CuHTaeBpy_RT). Moreover, the collapse of the hydrogen bonds gives rise to a nearly ideal paramagnetic behavior with zero Weiss temperature for the dehydrated compound (CuHTaeBpy_HT).

ASSOCIATED CONTENT

Supporting Information

The Supporting Information is available free of charge on the ACS Publications website at DOI: 10.1021/acs.inorgchem.6b01199.

Graph of subgroups. Hydrogen bonding for the average structure. Powder X-ray diffraction refinements. Shape map for geometrical distortions. Thermogravimetry. Thermodiffractometry. Simplification of the Cu-Bpy metal−organic chains. Thermal evolution of the cell parameters. IR spectra. UV−vis spectra. X-band EPR spectra of the hydrated and anhydrous phases. Magnetic fitting to 1D and 2D models. (PDF)

X-ray crystallographic information (CIF)

X-ray crystallographic information (CIF)

AUTHOR INFORMATION

Corresponding Authors

*E-mail: roberto.fernandez@bcmaterials.net. (R.F.d.L.)

*E-mail: maribel.arriortua@ehu.eus. Phone: 34-946012162/2555. Fax: 34-946013500. (M.I.A.)

Notes

The authors declare no competing financial interest.

Crystallographic information files (CIF) have been deposited in the CSD (Cambridge Structural Database): Structure numbers: 1477960−1477961.

ACKNOWLEDGMENTS

This work has been financially supported by the European Regional Development Fund (ERDF), the "Ministerio de Economía y Competitividad" (MAT2013-42092-R), the "Gobierno Vasco" (Basque University Research System Group, IT-630-13 and Economic Development and Competitiveness, ACTIMAT and LISOL projects, ELKARTEK program, KK-2015/00094), UPV/EHU (UFI 11/15), which we gratefully acknowledge. The authors thank the technicians of SGIker (UPV/EHU). R.F.d.L. thanks BCMaterials for his contract. J.O. wishes to thank CONICYT for the 2015 FONDECYT postdoctoral project (No. 3150455).

REFERENCES

(1) (a) Bloch, W. M.; Champness, N. R.; Doonan, C. J. X-ray Crystallography in Open-Framework Materials. *Angew. Chem., Int. Ed.* **2015**, *54*, 12860−12867. (b) Burtch, N. C.; Jasuja, H.; Walton, K. S. Water stability and adsorption in metal-organic frameworks. *Chem. Rev.* **2014**, *114*, 10575−10612. (c) Cui, Y.; Li, B.; He, H.; Zhou, W.; Chen, B.; Qian, G. Metal-Organic Frameworks as Platforms for Functional Materials. *Acc. Chem. Res.* **2016**, *49*, 483−493. (d) Fernández de Luis, R.; Orive, J.; Larrea, E. S.; Karmele Urtiaga, M. K.; Arriortua, M. I. Hybrid vanadates constructed from extended metal - organic arrays: crystal architectures and properties. *CrystEngComm* **2014**, *16*, 10332−10366. (e) Devic, T.; Serre, C. High valence 3p and transition metal based MOFs. *Chem. Soc. Rev.* **2014**, *43*, 6097−6115. (f) Ezugwu, C. I.; Kabir, N. A.; Yusubov, M.;

DOI: 10.1021/acs.inorgchem.6b01199
Inorg. Chem. 2016, 55, 11662−11675

Verpoort, F. Metal−organic frameworks containing N-heterocyclic carbenes and their precursors. *Coord. Chem. Rev.* **2016**, *307*, 188−210.
(2) (a) Coronado, E.; Minguez Espallargas, G. Dynamic magnetic MOFs. *Chem. Soc. Rev.* **2013**, *42*, 1525−1539. (b) Grancha, T.; Mon, M.; Lloret, F.; Ferrando-Soria, J.; Journaux, Y.; Pasán, J.; Pardo, E. Double Interpenetration in a Chiral Three-Dimensional Magnet with a (10,3)-a Structure. *Inorg. Chem.* **2015**, *54*, 8890−8892. (c) Fernández de Luis, R.; Urtiaga, M. K.; Mesa, J. L.; Vidal, K.; Lezama, L.; Rojo, T.; Arriortua, M. I. Short-Range and Long-Range Magnetic Ordering, in Third Generation Brannerite Type Inorganic−Organic Vanadates: $[\{Mn(Bpy)\}(VO_3)_2]\approx(H_2O)_{1.16}$ and $[\{Mn(Bpy)_{0.5}\}(VO_3)_2]\approx(H_2O)_{0.62}$. *Chem. Mater.* **2010**, *22*, 5543−5553. (d) Larrea, E. S.; Mesa, J. L.; Pizarro, J. L.; Fernández de Luis, R.; Rodriguez Fernández, J.; Rojo, T.; Arriortua, M. I. Synthesis and comparative study of Co(pym) $(VO_3)_2$ and $[Co(H_2O)_2(VO_3)_2]\cdot 2H_2O$. *Dalton Trans.* **2012**, *41*, 14170−14179.
(3) (a) Hu, Z.; Deibert, B. J.; Li, J. Luminescent metal-organic frameworks for chemical sensing and explosive detection. *Chem. Soc. Rev.* **2014**, *43*, 5815−5840. (b) Kreno, L. E.; Leong, K.; Farha, O. K.; Allendorf, M.; Van Duyne, R. P.; Hupp, J. T. Metal-organic framework materials as chemical sensors. *Chem. Rev.* **2012**, *112*, 1105−1125. (c) Calderón-Casado, A.; Barandika, G.; Bazán, B.; Urtiaga, M. K.; Arriortua, M. I. Host−guest chemistry of Ni II coordination compounds with PDC and $(py)_2CO$: reversible crystal-to-amorphous transformations induced by solvent exchange. *CrystEngComm* **2013**, *15*, 5134.
(4) (a) Férey, G. Structural flexibility in crystallized matter: from history to applications. *Dalton Trans.* **2016**, *45* (10), 4073−4089. (b) Lin, Z.-J.; Lü, J.; Hong, M.; Cao, R. Metal−organic frameworks based on flexible ligands (FL-MOFs): structures and applications. *Chem. Soc. Rev.* **2014**, *43*, 5867−5895. (c) Calderón-Casado, A.; Barandika, G.; Bazán, B.; Urtiaga, M. K.; Vallcorba, O.; Rius, J.; Arriortua, M. I.; et al. Solid-state transformation of the MOF $[Ni_2(bipy)_{1.5}(PDC)_2(H_2O)_2]\cdot 3.5H_2O$. *CrystEngComm* **2011**, *13*, 6831−6838. (d) Fidalgo-Marijuan, A.; Barandika, G.; Bazán, B.; Urtiaga, M. K.; Arriortua, M. I. Thermal stability and crystallochemical analysis for CoII - based coordination polymers with TPP and TPPS porphyrins. *CrystEngComm* **2013**, *15*, 4181−4188. (e) Llano-Tomé, F.; Bazán, B.; Urtiaga, M. K.; Barandika, G.; Fidalgo-Marijuan, A.; Fernández de Luis, R.; Arriortua, M. I. Water-induced phase transformation of a Cu II coordination framework with pyridine-2,5-dicarboxylate and di-2-pyridyl ketone: synchrotron radiation analysis. *CrystEngComm* **2015**, *17*, 6346−6354.
(5) (a) Horike, S.; Umeyama, D.; Kitagawa, S. Ion conductivity and transport by porous coordination polymers and metal-organic frameworks. *Acc. Chem. Res.* **2013**, *46*, 2376−2384. (b) Ramaswamy, P.; Wong, N. E.; Shimizu, G. K. H. MOFs as proton conductors−challenges and opportunities. *Chem. Soc. Rev.* **2014**, *43*, 5913−5932. (c) Fernández de Luis, R.; Ponrouch, A.; Rosa Palacín, M.; Karmele Urtiaga, M. K.; Arriortua, M. I. Electrochemical behavior of $[\{Mn(Bpy)\}(VO_3)_2]\cdot(H_2O)_{1.24}$ and $[\{Mn(Bpy)_{0.5}\}(VO_3)2]\cdot(H_2O)_{0.62}$ inorganic−organic Brannerites in lithium and sodium cells. *J. Solid State Chem.* **2014**, *212*, 92−98.
(6) (a) Stavila, V.; Talin, A. A.; Allendorf, M. D. MOF-based electronic and opto-electronic devices. *Chem. Soc. Rev.* **2014**, *43*, 5994−6010. (b) Aguirre-Díaz, L. M.; Gándara, F.; Iglesias, M.; Snejko, N.; Gutiérrez-Puebla, E.; Monge, M. Á. Tunable Catalytic Activity of Solid Solution Metal−Organic Frameworks in One-Pot Multicomponent Reactions. *J. Am. Chem. Soc.* **2015**, *137*, 6132−6135. (c) Conde-González, J. E.; Peña-Méndez, E. M.; Rybáková, S.; Pasán, J.; Ruiz-Pérez, C.; Havel, J. Adsorption of silver nanoparticles from aqueous solution on copper-based metal organic frameworks (HKUST-1). *Chemosphere* **2016**, *150*, 659−666. (d) Larrea, E. S.; Fernández de Luis, R.; Orive, J.; Iglesias, M.; Arriortua, M. I. [NaCu(2,4-HPdc)(2,4-Pdc)] Mixed Metal-Organic Framework as a Heterogeneous Catalyst. *Eur. J. Inorg. Chem.* **2015**, *2015*, 4699−4707. (e) Grancha, T.; Ferrando-Soria, J.; Zhou, H.-C.; Gascon, J.; Seoane, B.; Pasán, J.; Pardo, E.; et al. Postsynthetic Improvement of the Physical Properties in a Metal-Organic Framework through a Single Crystal to Single Crystal Transmetallation. *Angew. Chem., Int. Ed.* **2015**, *54*, 6521−6525. (f) Wang, L.; Han, Y.; Feng, X.; Zhou, J.; Qi, P.; Wang, B. Metal−organic frameworks for energy storage: Batteries and supercapacitors. *Coord. Chem. Rev.* **2016**, *307*, 361−381. (g) Wang, S.; Wang, X. Multifunctional Metal−Organic Frameworks for Photocatalysis. *Small* **2015**, *11*, 3097−3112.
(7) (a) Thanasekaran, P.; Luo, T.-T.; Wu, J.-Y.; Lu, K.-L. Giant metal−organic frameworks with bulky scaffolds: from microporous to mesoporous functional materials. *Dalton Trans.* **2012**, *41*, 5437. (b) Sun, L.; Campbell, M. G.; Dincă, M. Electrically Conductive Porous Metal−Organic Frameworks. *Angew. Chem., Int. Ed.* **2016**, *55*, 3566−3579. (c) Fernández de Luis, R.; Mesa, J. L.; Urtiaga, M. K.; Lezama, L.; Arriortua, M. I.; Rojo, T. Topological description of a 3D self-catenated nickel hybrid vanadate Ni(bpe) $(VO_3)_2$. Thermal stability, spectroscopic and magnetic properties. *New J. Chem.* **2008**, *32*, 1582−1588. (d) Senkovska, I.; Kaskel, S. Ultrahigh porosity in mesoporous MOFs: promises and limitations. *Chem. Commun.* **2014**, *50*, 7089. (e) Schneemann, A.; Bon, V.; Schwedler, I.; Senkovska, I.; Kaskel, S.; Fischer, R. A. Flexible metal−organic frameworks. *Chem. Soc. Rev.* **2014**, *43*, 6062−6096. (f) Vardhan, H.; Yusubov, M.; Verpoort, F. Self-assembled metal-organic polyhedra: An overview of various applications *Coor. Coord. Chem. Rev.* **2016**, *306*, 171−194. (g) Castillo-Blas, C.; Snejko, N.; de la Peña-O'Shea, V. A.; Gallardo, J.; Gutiérrez-Puebla, E.; Monge, M. A.; Gándara, F. Crystal phase competition by addition of a second metal cation in solid solution metal−organic frameworks. *Dalton Trans.* **2016**, *45*, 4327−4337.
(8) (a) Zhou, H.-C.; Kitagawa, S. Metal−Organic Frameworks (MOFs). *Chem. Soc. Rev.* **2014**, *43*, 5415−5418. (b) Amayuelas, E.; Fidalgo-Marijuan, A.; Barandika, G.; Bazán, B.; Urtiaga, M. K.; Arriortua, M. I. Mother structures related to the hexagonal and cubic close packing in Cu_{24} clusters: solvent-influenced derivatives. *CrystEngComm* **2015**, *17*, 3297−3304. (c) Bravo-García, L.; Barandika, G.; Bazán, B.; Urtiaga, M. K.; Arriortua, M. I. Thermal stability of ionic nets with Cu II ions coordinated to di-2-pyridyl ketone: Reversible crystal-to-crystal phase transformation. *Polyhedron* **2015**, *92*, 117−123. (d) Fidalgo-Marijuan, A.; Barandika, G.; Bazan, B.; Urtiaga, M. K.; Lezama, L.; Arriortua, M. I. A Fe-TPP Coordination Network with Metalloporphyrinic Neutral Radicals and Face-to-Face and Edge-to-Face π-π Stacking. Inorganic Chemistry. *Inorg. Chem.* **2013**, *52*, 8074−8081.
(9) Guo, Q.; Merkens, C.; Si, R.; Englert, U. Crosslinking of the $Pd(acacCN)_2$ building unit with Ag(I) salts: dynamic 1D polymers and an extended 3D network. *CrystEngComm* **2015**, *17*, 4383−4393.
(10) (a) Dutta, S.; Biswas, P.; Dutta, S. K.; Nag, K. Methoxo-bridged diiron(III) complex of *m*-xylylenebis(acetylacetonate) showing remarkable thermal stability for encapsulated dichloromethane. *New J. Chem.* **2009**, *33*, 847−852. (b) Rancan, M.; Dolmella, A.; Seraglia, R.; Orlandi, S.; Quici, S.; Sorace, L.; Armelao, L.; et al. Dinuclear Cu(II) Complexes of Isomeric Bis-(3-acetylacetonate)benzene Ligands: Synthesis, Structure, and Magnetic Properties. *Inorg. Chem.* **2012**, *51*, 5409−5416.
(11) (a) Rancan, M.; Tessarolo, J.; Casarin, M.; Zanonato, P. L.; Quici, S.; Armelao, L. Double Level Selection in a Constitutional Dynamic Library of Coordination Driven Supramolecular Polygons. *Inorg. Chem.* **2014**, *53*, 7276−7287. (b) Rancan, M.; Dolmella, A.; Seraglia, R.; Orlandi, S.; Quici, S.; Armelao, L. A templating guest sorts out a molecular triangle from a dimer−trimer constitutional dynamic library. *Chem. Commun.* **2012**, *48*, 3115−3117. (c) Cherutoi, J. K.; Sandifer, J. D.; Pokharel, U. R.; Fronczek, F. R.; Pakhomova, S.; Maverick, A. W. Externally and Internally Functionalized Copper(II) β-Diketonate Molecular Squares. *Inorg. Chem.* **2015**, *54*, 7791−7802. (d) Liu, T.; Liu, Y.; Xuan, W.; Cui, Y. Chiral Nanoscale Metal−Organic Tetrahedral Cages: Diastereoselective Self-Assembly and Enantioselective Separation. *Angew. Chem., Int. Ed.* **2010**, *49*, 4121−4124.
(12) Pariya, C.; Fronczek, F. R.; Maverick, A. W. Bis(*o*-phenylenebis-(acetylacetonato))dicopper(II): A Strained Copper(II) Dimer Exhibiting a Wide Range of Colors in the Solid State. *Inorg. Chem.* **2011**, *50*, 2748−2753.

DOI: 10.1021/acs.inorgchem.6b01199
Inorg. Chem. 2016, 55, 11662−11675

(13) (a) Tsiamis, C.; Hatzidimitriou, A. G.; Tzavellas, L. C. Influence of the Bridging Group of Cross-Conjugated Nitrogenous Bases on the Spectra and Structure of Solvatochromic Mixed-Ligand Copper(II) Chelates Containing β-Ketoenols. *Inorg. Chem.* **1998**, *37*, 2903−2909. (b) Chen, B.; Fronczek, F. R.; Maverick, A. W. 3-(4-Cyanophenyl)-pentane-2,4-dione and its copper(II) complex. *Acta Crystallogr., Sect. C: Cryst. Struct. Commun.* **2004**, *60*, m147−m149. (c) Voutsas, G.; Tzavellas, L. C.; Tsiamis, C. Self-Assemblies and Supramolecular Structures in Metal β-Dionates: Crystal and Molecular Structure of Bis(aquo)bis(3-cyano-2,4-pentanedionato)zinc(II) Dihydrate, $[Zn(H_2O)_2(NC\text{-}acac)_2]\cdot 2H_2O$. *Struct. Chem.* **1999**, *10*, 53−57. (c1) Chen, B.; Fronczek, F. R.; Maverick, A. W. Solvent-dependent 4^4 square grid and $6^4.8^2$ NbO frameworks formed by $Cu(Pyac)_2$ (bis[3-(4-pyridyl)pentane-2,4-dionato]copper(II)). *Chem. Commun.* **2003**, 2166−2167. (d) Turner, S. S.; Collison, D.; Mabbs, F. E.; Halliwell, M. Preparation, magnetic properties and crystal structure of bis[3-(4-pyridyl)pentane-2,4-dionato]copper(II). *J. Chem. Soc., Dalton Trans.* **1997**, 1117−1118. (e) Yoshida, J.; Nishikiori, S.; Kuroda, R.; Yuge, H. Three Polymorphic Cd^{II} Coordination Polymers Obtained from the Solution and Mechanochemical Reactions of 3-Cyanopentane-2,4-dione with Cd^{II} Acetate. *Chem. - Eur. J.* **2013**, *19*, 3451−3457. (f) Sakamoto, H.; Matsuda, R.; Bureekaew, S.; Tanaka, D.; Kitagawa, S. A Porous Coordination Polymer with Accessible Metal Sites and its Complementary Coordination Action. *Chem. - Eur. J.* **2009**, *15*, 4985−4989.

(14) (a) Chen, B.; Fronczek, F. R.; Maverick, A. W. Porous Cu−Cd Mixed-Metal−Organic Frameworks Constructed from $Cu(Pyac)_2$ {Bis[3-(4-pyridyl)pentane-2,4-dionato]copper(II)}. *Inorg. Chem.* **2004**, *43*, 8209−8211. (b) Kilduff, B.; Pogozhev, D.; Baudron, S. A.; Hosseini, M. W. Heterometallic Architectures Based on the Combination of Heteroleptic Copper and Cobalt Complexes with Silver Salts. *Inorg. Chem.* **2010**, *49*, 11231−11239. (c) Vreshch, V. D.; Lysenko, A. B.; Chernega, A. N.; Howard, J. A. K.; Krautscheid, H.; Sieler, J.; Domasevitch, K. V. Extended coordination frameworks incorporating heterobimetallic squares. *Dalton Trans.* **2004**, 2899−2903. (d) Kondracka, M.; Englert, U. Bimetallic Coordination Polymers via Combination of Substitution-Inert Building Blocks and Labile Connectors. *Inorg. Chem.* **2008**, *47*, 10246−10257. (e) Burrows, A. D.; Cassar, K.; Mahon, M. F.; Warren, J. E. The stepwise formation of mixed-metal coordination networks using complexes of 3-cyanoacetylacetonate. *Dalton Trans.* **2007**, 2499−2509.

(15) (a) Burrows, A. D.; Cassar, K.; Mahon, M. F.; Rigby, S. P.; Warren, J. E. Synthesis and characterisation of metal−organic frameworks containing bis(β-diketonate) linkers. *CrystEngComm* **2008**, *10*, 1474. (b) Yang, Q.; Tan, X.; Wang, S.; Zhang, J.; Chen, L.; Zhang, J.-P.; Su, C.-Y. Porous organic−inorganic hybrid aerogels based on bridging acetylacetonate. *Microporous Mesoporous Mater.* **2014**, *187*, 108−113.

(16) (a) Zhang, Y.; Wang, S.; Enright, G. D.; Breeze, S. R. Tetraacetylethane Dianion (Tae) As a Bridging Ligand for Molecular Square Complexes: $Co^{II}_4(Tae)_4(Dpa)_4$, Dpa = Di-2-pyridylamine, a Chiral Molecular Square in the Solid State. *J. Am. Chem. Soc.* **1998**, *120*, 9398−9399. (b) Tovilla, J. A.; Hernández-Ortega, S.; Valdés-Martínez, J. (3,4-Diacetylhexa-2,4-diene-2,5-diolato-$^4O^2$,O^3:O^4,O^5)bis-[aqua(1,10-phenanthroline-*N*,*N*′)copper(II)]bis(tetrafluoridoborate) monohydrate. *Acta Crystallogr., Sect. E: Struct. Rep. Online* **2009**, *65*, m366−m367. (c) Lambert, J. B.; Liu, Z. Dinuclear Complexes and a One-dimensional Chain Involving Difunctional Ligands Containing the Acetylacetonate Functionality. *J. Chem. Crystallogr.* **2007**, *37*, 629−639.

(17) Luisi, B. S.; Kravtsov, V. C.; Moulton, B. D. An (8,3)-a 3D Coordination Network and Concomitant Three-Connected Supramolecular Isomers. *Cryst. Growth Des.* **2006**, *6*, 2207−2209.

(18) Cepeda, J.; Balda, R.; Beobide, G.; Castillo, O.; Fernández, J.; Luque, A.; Vallejo-Sánchez, D.; et al. Lanthanide(III)/Pyrimidine-4,6-dicarboxylate/Oxalate Extended Frameworks: A Detailed Study Based on the Lanthanide Contraction and Temperature Effects. *Inorg. Chem.* **2011**, *50*, 8437−8451.

(19) (a) Gągor, A.; Węcławik, M.; Bondzior, B.; Jakubas, R. Periodic and incommensurately modulated phases in a (2-methylimidazolium)-tetraiodobismuthate(III) thermochromic organic−inorganic hybrid. *CrystEngComm* **2015**, *17*, 3286−3296.

(20) Chernyshov, D.; Hostettler, M.; Törnroos, K. W.; Bürgi, H.-B. Ordering Phenomena and Phase Transitions in a Spin-Crossover Compound—Uncovering the Nature of the Intermediate Phase of [Fe(2-pic)3]Cl2·EtOH. *Angew. Chem., Int. Ed.* **2003**, *42*, 3825−3830.

(21) Siegler, M.; Parkin, S.; Brock, C. P. $[Ni(MeCN)(H_2O)_2(NO_3)_2]\cdot$(15-crown-5)·MeCN: detailed study of a four-phase sequence that includes an intermediate modulated phase. *Acta Crystallogr., Sect. B: Struct. Sci.* **2012**, *68*, 389−400.

(22) (a) Banerjee, D.; Wang, H.; Gong, Q.; Plonka, A. M.; Jagiello, J.; Wu, H.; Woerner, W. R.; Emge, T. J.; Olson, D. H.; Parise, J. B.; Li, J. Direct structural evidence of commensurate-to-incommensurate transition of hydrocarbon adsorption in a microporous metal organic framework. *Chem. Sci.* **2016**, *7*, 759−765. (b) Wang, H.; Yao, K.; Zhang, Z.; Jagiello, J.; Gong, Q.; Han, Y.; Li, J. The first example of commensurate adsorption of atomic gas in a MOF and effective separation of xenon from other noble gases. *Chem. Sci.* **2014**, *5*, 620−624. (c) Liu, Z.; Nobuhisa, F.; Terasaki, O.; Ohsuna, T.; Hiraga, K.; Camblor, M. A.; Cheetham, A. K.; et al. Incommensurate Modulation in the Microporous Silica SSZ-24. *Chem. - Eur. J.* **2002**, *8*, 4549−4556.

(23) (a) Fernández de Luis, R.; Urtiaga, M. K.; Mesa, J. L.; Larrea, E. S.; Rojo, T.; Arriortua, M. I. Compositional space diagrams and crystallization sequences in M/Bpa/NaVO3 (M = Ni, Co) systems. Physical properties of $\{Ni(H_2O)(Bpa)\}(VO_3)_2$ center dot 2H(2)O and $\{Co(Bpa)\}(VO_3)_2$ 3D hybrid vanadates. *CrystEngComm* **2012**, *14*, 6921−6933. (b) Orive, J.; Larrea, E. S.; Fernández de Luis, R.; Iglesias, M.; Mesa, J. L.; Rojo, T.; Arriortua, M. I. Amine templated open-framework vanadium(III) phosphites with catalytic properties. *Dalton Trans.* **2013**, *42*, 4500−4512. (c) Fernández de Luis, R.; Mesa, J. L.; Urtiaga, M. K.; Larrea, E. S.; Rojo, T.; Arriortua, M. I. Flexible and Dynamic Thermal Behavior of Self-Catenated $[\{Ni_3(H_2O)_3(Bpa)_4\}(V_6O_{18})]\cdot 8H_2O$ Constructed from 10-c Heterometallic Inorganic−Organic Clusters. *Inorg. Chem.* **2012**, *51*, 2130−2139. (d) Fernández de Luis, R.; Urtiaga, M. K.; Mesa, J. L.; Aguayo, A. T.; Rojo, T.; Arriortua, M. I. Four nodal self-catenated $[\{Ni_8(Bpy)_{16}\}V_{24}O_{68}]\cdot 8.5(H_2O)$, combining three dimensional metal−organic and inorganic frameworks. *CrystEngComm* **2010**, *12*, 1880−1886.

(24) (a) Steiner, T. The hydrogen bond in the solid state. *Angew. Chem., Int. Ed.* **2002**, *41*, 48−76. (b) Fernández de Luis, R.; Urtiaga, M. K.; Mesa, J. L.; Larrea, E. S.; Rojo, T.; Arriortua, M. I.; et al. Thermal Response, Catalytic Activity, and Color Change of the First Hybrid Vanadate Containing Bpe Guest Molecules. *Inorg. Chem.* **2013**, *52*, 2615−2626.

(25) Desplanches, C.; Ruiz, E.; Rodríguez-Fortea, A.; Alvarez, S. Exchange Coupling of Transition-Metal Ions through Hydrogen Bonding: A Theoretical Investigation. *J. Am. Chem. Soc.* **2002**, *124*, 5197−5205.

(26) *CrysAlis RED*, version 1.171.33.55; Oxford Diffraction: Wroclaw, Poland, 2010.

(27) Yinghua, W. Lorentz-polarization factor for correction of diffraction-line profiles. *J. Appl. Crystallogr.* **1987**, *20*, 258−259.

(28) Altomare, A.; Cascarano, G.; Giacovazzo, C.; Guagliardi, A. Completion and refinement of crystal structures with *SIR*92. *J. Appl. Crystallogr.* **1993**, *26*, 343−350.

(29) (a) Sheldrick, G. M. *SHELX97*, Programs for Crystal Structure Analysis; Institüt für Anorganische Chemie der Universität: Göttingen, Germany, 1998.

(30) Farrugia, L. J. *WinGX* suite for small-molecule single-crystal crystallography. *J. Appl. Crystallogr.* **1999**, *32*, 837−838.

(31) Han, T. *International Tables for X-ray Crystallography;* Kynoch Press: Birmingham, UK, 1973, Vol. *4*.

(32) Rodríguez-Carvajal, J. Recent advances in magnetic structure determination by neutron powder diffraction. *Phys. B* **1993**, *192*, 55−69.

(33) Stokes, H. T.; Campbell, B. J.; van Smaalen, S. Generation of (3 + *d*)-dimensional superspace groups for describing the symmetry of

DOI: 10.1021/acs.inorgchem.6b01199
Inorg. Chem. 2016, 55, 11662−11675

modulated crystalline structures. *Acta Crystallogr., Sect. A: Found. Crystallogr.* **2011**, *67*, 45−55.
(34) (a) Mukherjee, R. *Comprehensive Coordination Chemistry II* **2003**, 747−910. (b) Noro, S. Rational synthesis and characterization of porous Cu(II) coordination polymers. *Phys. Chem. Chem. Phys.* **2010**, *12*, 2519−2531.
(35) (a) Brown, I. D. *Structure and Bonding in Crystals;* O'Keeffe, M., Navrotsky, A., Eds.; Academic Press: New York, 1981; Vol. 2. (b) Brese, N. S.; O'Keeffe, M. Bond-Valence Parameters for Solids. *Acta Crystallogr., Sect. B: Struct. Sci.* **1991**, *47*, 192−197. (c) Brown, I. D.; Altermatt, D. Bond-valence parameters obtained from a systematic analysis of the Inorganic Crystal Structure Database. *Acta Crystallogr., Sect. B: Struct. Sci.* **1985**, *B41*, 244−247.
(36) Llunell, M.; Casanova, D.; Cirera, J.; Alemany, P.; Alvarez, S. *Shape,* Program for the Stereochemical Analysis of Molecular Fragments by Means of Continuous Shape Measures and Associated Tools; Departament de Química Física, Departament de Química Inorgànica, and Institut de Química Teòrica i Computacional, Universitat de Barcelona: Barcelona, 2013.
(37) Lou, B.-Y.; Jiang, F.-L.; Wu, B.-L.; Yuan, D.-Q.; Hong, M.-C. From Helical Array to Porous Architecture: Exploring the Use of Side Chains of Amino Acids to Engineer 1D Infinite Coordination Polymeric Chain into Porous Frameworks. *Cryst. Growth Des.* **2006**, *6*, 989−993.
(38) Hu, R.-F.; Kang, Y.; Zhang, J.; Li, Z. J.; Qin, Y.-Y.; Yao, Y.-G. Three Copper(II) Coordination Polymers Constructed by Both Rigid and Flexible Ligands. *Z. Anorg. Allg. Chem.* **2005**, *631*, 3053−3057.
(39) Fan, G.; Xie, G.; Chen, S.; Gao, S. Water tape stabilized in a 3D porous copper(I) supramolecular network. *J. Coord. Chem.* **2007**, *60*, 1093−1099.
(40) Wang, R.; Jiang, F.; Zhou, Y.; Han, L.; Hong, M. Syntheses and characterizations of four mixed-ligand hydrogen bonding supramolecular architectures with different structural motifs. *Inorg. Chim. Acta* **2005**, *358*, 545−554.
(41) Zhong, K. L.; Chen, L.; et al. Poly[diaquabis(μ-4,4′-bipyridine-κ^2N:N')bis(ethane-1,2-diol)di-μ-sulfato-dicopper(II)]. *Acta Crystallogr., Sect. C: Cryst. Struct. Commun.* **2011**, *67*, m62−m64.
(42) (a) Fernández de Luis, R.; Orive, J.; Larrea, E. S.; Urtiaga, M. K.; Arriortua, M. I. Reversible Solid-State Transformation in $\{Ni_2(H_2O)_2(Bpa)_2\}(V_6O_{17})$ Proved by Synchrotron Radiation: Color and Magnetic Properties Change. *Cryst. Growth Des.* **2014**, *14*, 658−670. (b) Llano-Tomé, F.; Bazán, B.; Urtiaga, M.-K.; Barandika, G.; Lezama, L.; Arriortua, M. I. Cu II−PDC-bpe frameworks (PDC= 2, 5-pyridinedicarboxylate, bpe= 1, 2-di (4-pyridyl) ethylene): mapping of herringbone-type structures. *CrystEngComm* **2014**, *16*, 8726. (c) Fernández de Luis, R.; Mesa, J. L.; Karmele Urtiaga, M.; Rojo, T.; Arriortua, M. I. Two Self-Catenated Nickel(II) Hybrid Vanadates with Honeycomb-Like 3DInorganic Frameworks Stabilized by Crossed Organic Bpe Pillars: Thermal, Spectroscopic and Magnetic Properties. *Eur. J. Inorg. Chem.* **2009**, *2009*, 4786−4794.
(43) (a) Goodwin, A. L.; Kepert, C. Negative thermal expansion and low-frequency modes in cyanide-bridged framework materials. *Phys. Rev. B: Condens. Matter Mater. Phys.* **2005**, *B71*, 1−4. (b) Goodwin, A. L.; Calleja, M.; Conterio, M. J.; Dove, M. T.; Evans, J. S.O.; Keen, D. A.; Peters, L.; Tucker, M. G. Colossal positive and negative thermal expansion in the framework material $Ag_3[Co(CN)_6]$. *Science* **2008**, *319*, 794−797. (c) Korčok, J. L.; Katz, M. J.; Leznoff, D. B. Impact of Metallophilicity on "Colossal" Positive and Negative Thermal Expansion in a Series of Isostructural Dicyanometallate Coordination Polymers. *J. Am. Chem. Soc.* **2009**, *131*, 4866−4871.
(44) (a) Dubbeldam, D.; Walton, K. S.; Ellis, D. E.; Snurr, R. Exceptional Negative Thermal Expansion in Isoreticular Metal−Organic Frameworks. *Angew. Chem., Int. Ed.* **2007**, *46*, 4496−4499. (b) Peterson, V. K.; Kearley, G. J.; Wu, Y.; Ramírez-Cuesta, A. J.; Kemner, E.; Kepert, C. J. anic Frameworks Local Vibrational Mechanism for Negative Thermal Expansion: A Combined Neutron Scattering and First-Principles Study. *Angew. Chem., Int. Ed.* **2010**, *49*, 585−588.
(45) Hathaway, B. J.; Billing, D. The electronic properties and stereochemistry of mono-nuclear complexes of the copper(II) ion. *Coord. Chem. Rev.* **1970**, *5*, 143−207.
(46) (a) Meyer, A.; Schnakenburg, G.; Glaum, R.; Schiemann, O. (Bis(terpyridine))copper(II) Tetraphenylborate: A Complex Example for the Jahn−Teller Effect. *Inorg. Chem.* **2015**, *54*, 8456−8464. (b) Jiang, Y.-M.; Yin, Z.; He, K.-H.; Zeng, M.-H.; Kurmoo, M. Reversible Shuttle Action upon Dehydration and Rehydration Processes in Cationic Coordinatively-Bonded (4,4) Square-Grid Nets Threaded by Supramolecular Bonded Anions, $\{[Cu^{II}(4,4'\text{-bpy})_2(H_2O)][Cu^{II}(2\text{-py}SO_3)_3](NO_3)\}\cdot H_2O$. *Inorg. Chem.* **2011**, *50*, 2329−2333.
(47) (a) Cortés, R.; Lezama, L.; Larramendi, J. I. R.; Insausti, M.; Folgado, J. V.; Madariaga, G.; Rojo, T. Crystal structure, spectroscopic and magnetic properties of two unusual compounds: $[Cu(terpy)(N_3)\text{-}Cl]$ and $[\{Cu_{0.75}Ni_{0.25}(terpy)(N_3)_2\}_2]\cdot 2H_2O$ (terpy = 2,2′: 6′,2″-terpyridine). *J. Chem. Soc., Dalton Trans.* **1994**, 2573−2579. (b) Caballero, A. B.; Rodríguez-Diéguez, A.; Lezama, L.; Barea, E.; Salas, J. M. Structural and magnetic properties of three novel complexes with the versatile ligand 5-methyl-1,2,4-triazolo[1,5-*a*]-pyrimidin-7(4H)-one. *Dalton Trans.* **2011**, *40*, 5180−5187.
(48) Hughes, R. C.; Morosin, B.; Richards, P. M.; et al. Electron spin resonance and structure of magnetically inequivalent chains in CuCl2·2NC5H5. *Phys. Rev. B* **1975**, *11*, 1795.
(49) (a) Carlin, R. L. *Magnetochemistry;* Springer-Verlag: Berlin, Germany, 1986,. (b) Fadaee, F.; Amirnasr, M.; Prša, K.; Pattison, P.; Shaik, N. E.; Rønnow, H. M.; Esrafili, M. D.; Omrani, A.; Amiri, A.; Schenk-Joß, K. Intrachain anti-ferromagnetic exchange in a 1D branched-chain built of two different copper(II) centres interlinked by end-on azido and phenoxo bridges: electron density map, electrochemical and magnetic properties. *RSC Adv.* **2015**, *5*, 59926−59934. (c) Bulut, A.; Topkaya, R.; Aktaş, B.; Doğan, S.; Kurt, H.; Yücesan, G.; Zorlu, B. Y. Macrocyclic Cu(II)-organophosphonate building block with room temperature magnetic ordering. *Dalton Trans.* **2015**, *44*, 12526−12529.
(50) Okazawa, A.; Ishida, T. Super−superexchange coupling through a hydrogen bond in a linear copper(II) complex, $[Cu(LH)(L)]\cdot BF_4\cdot 2H_2O$ (LH = *N*-*tert*-butyl-*N*-2-pyridylhydroxylamine). *Chem. Phys. Lett.* **2009**, *480*, 198−202.
(51) (a) Cortijo, M.; González-Prieto, R.; Herrero, S.; Jiménez-Aparicio, R.; Sánchez-Rivera, P. Ferromagnetic Interactions through Hydrogen Bonds in a One-Dimensional Ni^{II} Coordination Polymer. *Eur. J. Inorg. Chem.* **2013**, *2013*, 5523−5527. (b) Bakalbassis, E. G.; Korabik, M.; Michailides, A.; Mrozinski, J.; Raptopoulou, C.; Skoulika, S.; Terzis, A.; Tsaousis, D. Crystal architecture and magnetic properties of four transition-metal adipate coordination polymers. *J. Chem. Soc., Dalton Trans.* **2001**, 850−857. (c) Ji, C.-C.; Li, J.; Guo, Y.-Z.; Zheng, Z.-J.; Li, Y. Eight new complexes based on flexible multicarboxylate ligands: synthesis, structures and properties. *CrystEngComm* **2010**, *12*, 3183−3194.
(52) Escrivá, E.; Server-Carrió, J.; García-Lozano, J.; Folgado, J. V.; Sapina, F.; Lezama, L. Exchange interactions through hydrogen-bond bridges. Crystal structure, spectroscopic characterisation and magnetic properties of the complex $[\{Cu(en)\}_2(\mu\text{-egta})]\cdot 4H_2O$ (H_4egta = 3,12-bis(carboxymethyl)-6,9-dioxa-3,12-diazatetradecanedionic acid). *Inorg. Chim. Acta* **1998**, *279*, 58−64.

DOI: 10.1021/acs.inorgchem.6b01199
Inorg. Chem. 2016, 55, 11662−11675